Supporting Information

Amphiphilic Perylene Bisimide-Polymer Conjugates by Cysteine-Based Orthogonal Strategy: Vesicular Aggregation, DNA Binding, and Cell Imaging

Mahuya Kar[a], Md. Anas[#a], Palash Banerjee[#a], Arpana Singh[b], Prosenjit Sen[b], and Tarun K. Mandal*[a]

[a]*School of Chemical Sciences, Indian Association for the Cultivation of Science, Jadavpur, Kolkata 700032, India*

[b]*School of Biological Sciences, Indian Association for the Cultivation of Science, Jadavpur, Kolkata 700032, India*

Email: psutkm@iacs.res.in

Contents **Page No.**

Table S1.	Molecular weight characterization and polymerization conditions	S3
Figure S1.	FTIR spectra of PDA, **Cys-PVim-I** and **PBI-(Cys-PVim-I)$_2$**	S4
Figure S2.	^{1}H-NMR spectrum of **Cys-PVim-I**	S5
Figure S3.	MALDI-TOF-MS spectrum of **Cys-PVim-I**	S6
Figure S4.	FTIR spectra of **Cys-PVim-II** and **PBI-(Cys-PVim-II)$_2$**	S7
Figure S5.	^{1}H-NMR spectrum of **Cys-PVim-II**	S8
Molecular weight determination of Cys-PVim from ^{1}H-NMR spectrum		S9
Figure S6.	MALDI-TOF-MS spectrum of **Cys-PVim-II**	S10
Figure S7.	^{1}H-NMR spectrum of **PBI-(Cys-PVim-I)$_2$**	S11
Figure S8.	^{13}C-NMR spectrum of **PBI-(Cys-PVim-I)$_2$**	S12
Figure S9.	^{1}H-NMR spectrum of **PBI-(Cys-PVim-II)$_2$**	S13
Figure S10.	Concentration variation UV-vis spectra of ctDNA	S14
Figure S11.	SEC chromatographs of PBI-(Cys-PVim)$_2$ conjugates	S15
Figure S12.	Emission spectra of **PBI-(Cys-PVim-II)$_2$** at different excitation.	S16
Figure S13.	Images of **PBI-(Cys-PVim-II)$_2$** under ambient light and UV lamp	S17
Table S2.	Quantum yield (ϕ) measurements of PBI-(Cys-PVim)$_2$	S18
Figure S14.	Concentration-dependent UV-vis spectra of **PBI-(Cys-PVim-I)$_2$**	S19
Figure S15.	Concentration-dependent emission spectra of **PBI-(Cys-PVim-I)$_2$**	S20

Scheme S1.	Aggregation of PBI-(Cys-PVim)$_2$ conjugates under acidic medium	S21
Figure S16.	^{1}H-NMR spectrum of **PBI-(Cys-PVim-II)$_2$** in D_2O in presence of HCl	S22
Figure S17.	pH variation images of **PBI-(Cys-PVim-II)$_2$** under ambient and UV light	S23
Figure S18.	pH variation UV-Vis and emission spectra of **PBI-(Cys-PVim-I)$_2$**	S24
Figure S19.	D_h vs pH plot of the aqueous solution of **PBI-(Cys-PVim-II)$_2$**	S25
Figure S20.	D_h vs pH plot of the aqueous solution of **PBI-(Cys-PVim-I)$_2$**	S26
Figure S21.	DLS curves of **PBI-(Cys-PVim-I)$_2$** and **PBI-(Cys-PVim-II)$_2$**	S27
Figure S22.	CAC measurement plots of **PBI-(Cys-PVim-I)$_2$**	S28
Figure S23.	DLS curves of **PBI-(Cys-PVim-II)$_2$** in water at different time intervals	S29
Figure S24.	FESEM image of **PBI-(Cys-PVim-II)$_2$**	S30
Figure S25.	TEM images of aggregated **PBI-(Cys-PVim-I)$_2$/PBI-(Cys-PVim-II)$_2$**	S31
Figure S26.	Confocal images of aggregated **PBI-(Cys-PVim-I)$_2$/PBI-(Cys-PVim-II)$_2$**	S32
Figure S27.	Time-dependent fluorescence microscopic live cell imaging of HeLa cells	S33
Figure S28.	Mean fluorescence intensity vs time plot of incubated HeLa cells	S34
Figure S29.	pH-dependent fluorescence microscopy live cell imaging of HeLa cells	S35
Figure S30.	Mean fluorescence intensity vs pH plot of incubated HeLa cells	S36
Figure S31.	Zeta potential (ξ) curve of **PBI-(Cys-PVim-II)$_2$** in water	S37
Scheme S2.	Binding of ctDNA with PBI-(Cys-PVim)$_2$ conjugate	S38
Figure S32.	DLS plot of **PBI-(Cys-PVim-II)$_2$** at different concentrations of ctDNA	S39
Figure S33.	Gel image of PBI-(Cys-PVim)$_2$-ctDNA polyplex	S40
Figure S34.	Gel image of PBI-(Cys-PVim)$_2$-Plasmid DNA polyplex	S41
Figure S35.	ITC measurement plot of ctDNA with **PBI-(Cys-PVim-II)$_2$**	S42

Table S1. Molecular weight characterization and polymerization conditions of the different Cys-PVims and perylene bisimide-polymer conjugates.

Polymer	**$[M]_0/[I]_0$**	**$M_{n,\,theo}$ (Da)**	**$M_{n,\,H\text{-}NMR}$ (Da)**	**$M_{n,\,MALDI}$ (Da)**	**$M_{n,\,GPC}$ (Da)**	**Dispersity ($Đ$)**
Cys-PVim-I	10	1060	1400	1640[a]	1200[c]	1.17[a]
Cys-PVim-II	20	2000	2200	2400[a]	2500[c]	1.14[a]
PBI-(Cys-PVim-I)$_2$	-	2500	3200[e]	3600[d]	2800[b]	1.64[b]
PBI-(Cys-PVim-II)$_2$	-	4400	4700[e]	5100[d]	5400[b]	1.67[b]

Condition for polymerization: Solvent = Water; Time =24 h; Temperature = 70 °C.

$M_{n,\,theo} = [Vim]_0 \times M_{Vim}/[Cys]_0 + M_{Cys}$

[a]Data obtained from MALDI-TOF-MS analysis.

[b]Data obtained from SEC analysis.

[c]Unable to measured directly from SEC, but they were back calculated from the equation M_n of Cys-PVim = [$M_{n,\,GPC}$ of PBI-$(PVim)_2$ - M_{PBI}]/2.

[d]Unable to measured directly from MALDI-TOF-MS, but they were calculated from the equation: M_n of PBI-$(Cys\text{-}PVim)_2$ = [2×$M_{n,\,MALDI}$ of PVim + M_{PBI}].

[e]Calculated from the equation: M_n of PBI-$(Cys\text{-}PVim)_2$ = [2×$M_{n,\,HNMR}$ of PVim + M_{PBI}].

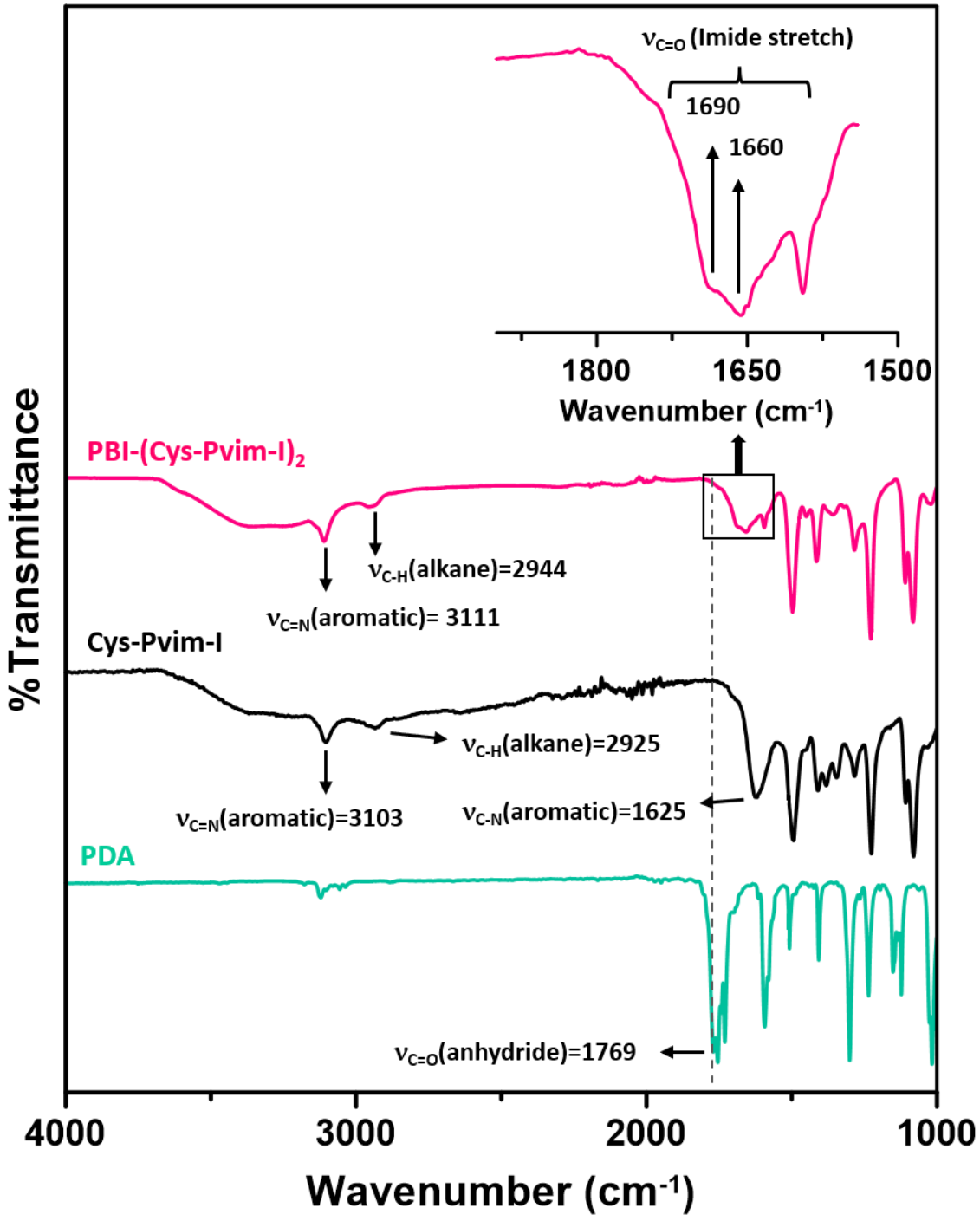

Figure S1. FTIR spectra of PDA, **Cys-PVim-I**, and **PBI-(Cys-PVim-I)$_2$** respectively.

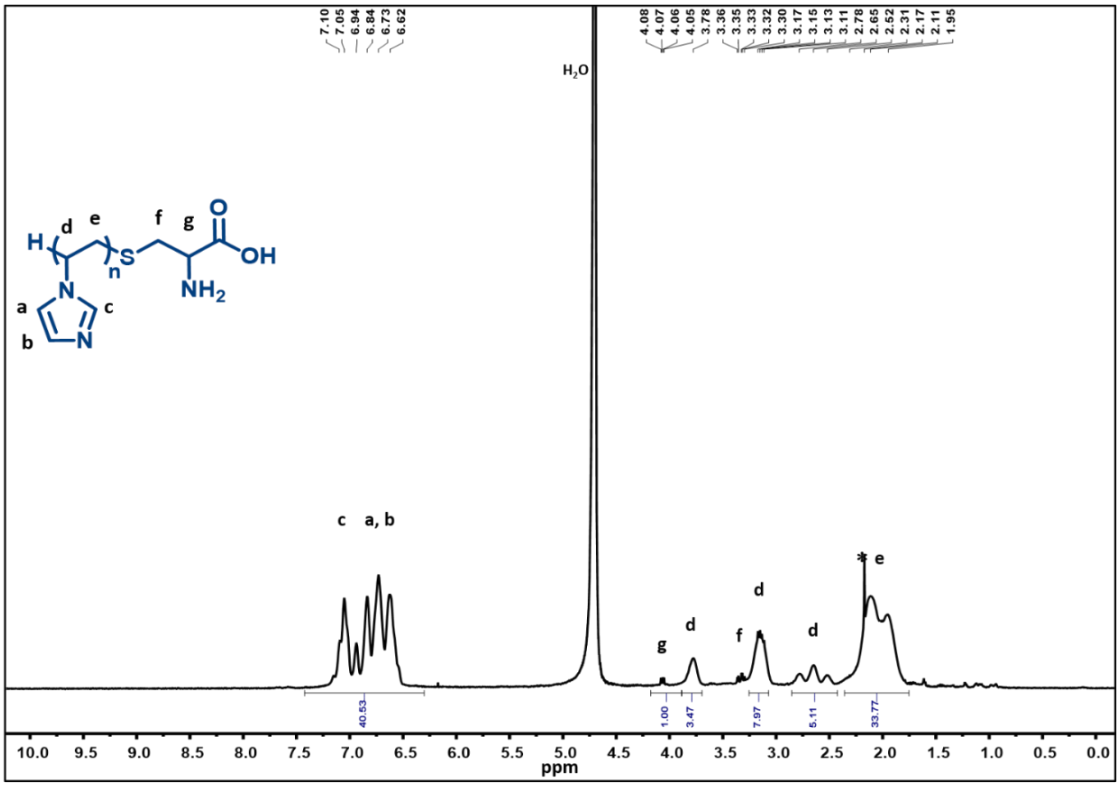

Figure S2. ^{1}H-NMR spectrum of **Cys-PVim-I** in D_2O (*acetone).

^{1}H-NMR (400 MHz, D_2O, TMS, δ ppm), Cys-PVim-I: 1.77-2.30 (-CH_2 of PVim backbone at position 'e'), 2.45-3.90 (-CH of PVim backbone at position 'd'), 3.36 (methylene proton of cysteine residue at position 'f'), 4.06 (methine proton of cysteine residue at position 'g'), 6.47-7.26 (imidazole ring protons at positions 'a', 'b' and 'c').

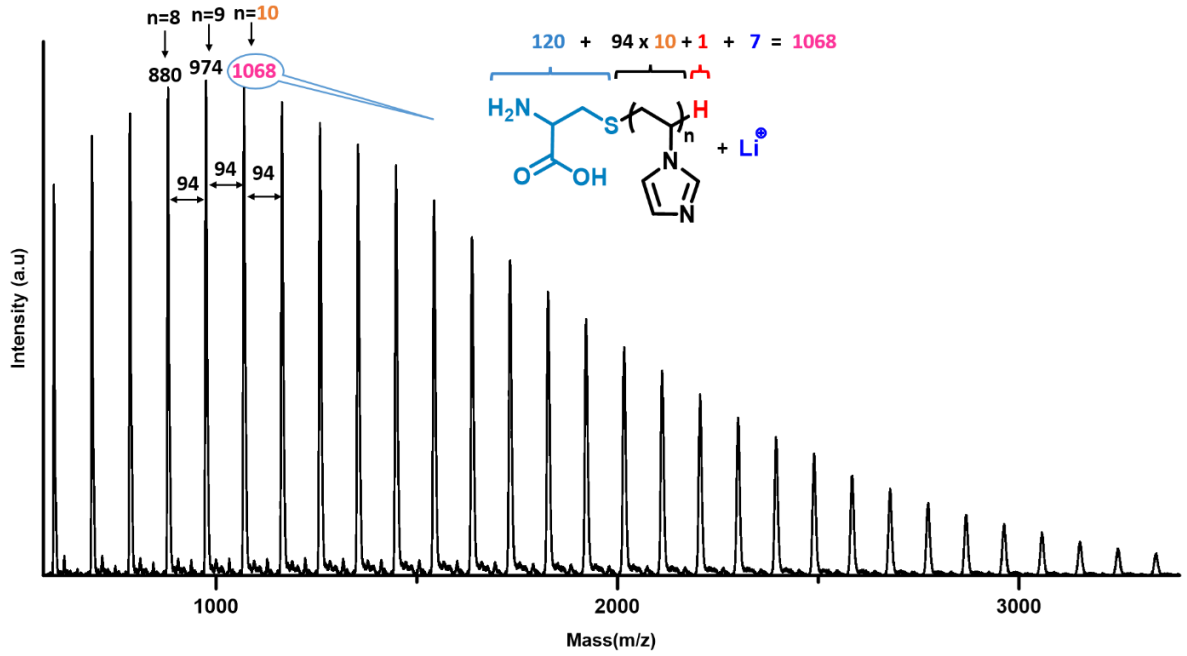

Figure S3. MALDI-TOF-MS spectrum of **Cys-PVim-I** in MeOH using DHB matrix and NaI.

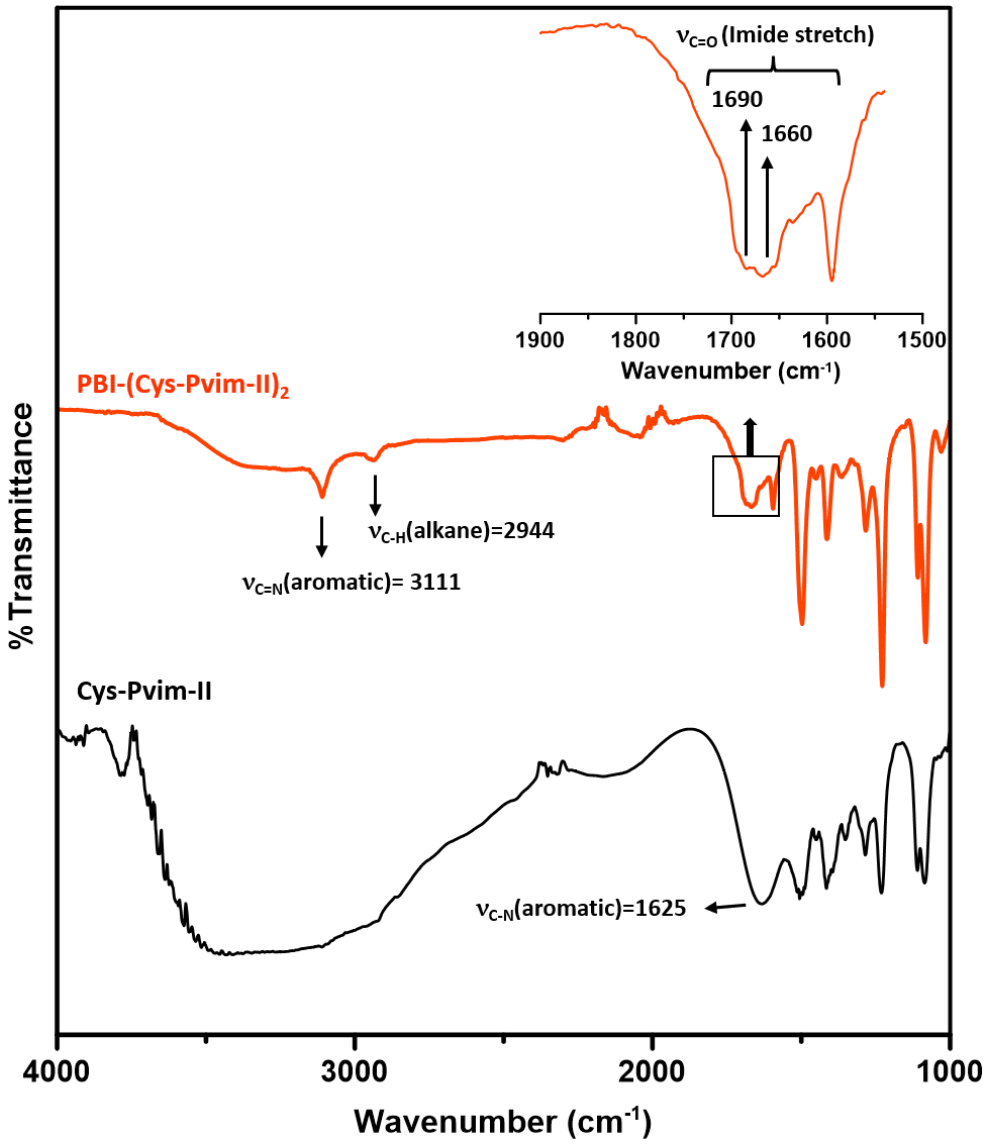

Figure S4. FTIR spectra of **Cys-PVim-II** and **PBI-(Cys-PVim-II)**$_2$ conjugate**.**

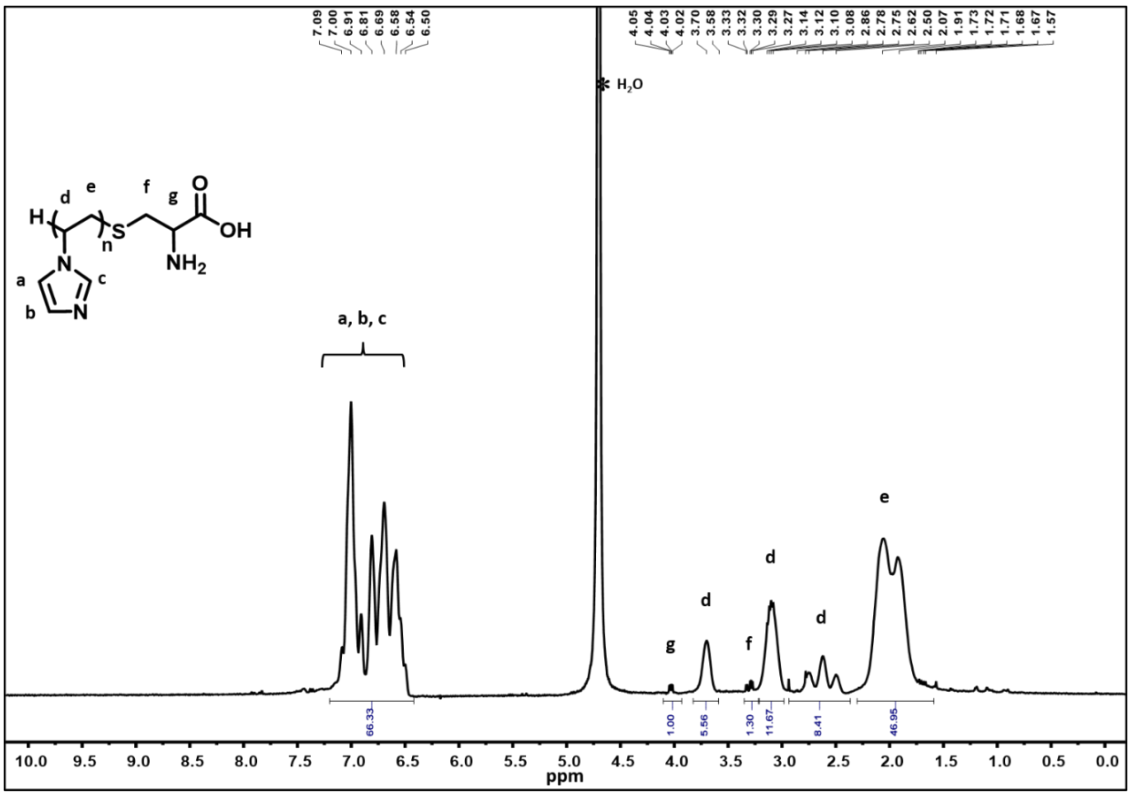

Figure S5. [1]H-NMR spectrum of **Cys-PVim-II** in D_2O.

[1]H-NMR (400 MHz, D_2O, TMS, δ ppm), Cys-PVim-II: 1.61-2.30 (-CH_2 of PVim backbone at position 'e'), 2.41-3.81 (-CH of PVim backbone at position 'd'), 3.28 (methylene proton of cysteine residue at position 'f'), 4.01 (methine proton of cysteine residue at position 'g'), 6.41-7.19 (imidazole ring protons at positions 'a', 'b' and 'c').

Molecular weight determination from end group analysis.

Comparing the integration area (see Figure S2) of the 'g' proton at ~ δ 4.06 ppm and the imidazole protons ('a', 'b' and 'c') at ~δ 6.47-7.26 ppm of the ^{1}H-NMR spectrum of **Cys-PVim-I** degree of polymerization (DP) was calculated by using the following equation.

DP = Int. of the repeating unit/N_o of repeating unit × N_o of the end group/Int. of the end group

= 40.53/3 × 1/1

= 13.51 ≈ 14

Molecular weight (M_n) of **Cys-PVim-I =** (14 × 94.05) + 120 + 1 = 1437.7 ≈ 1400 Da

Int. = Integration area, N_o = Number of protons, Molecular weight of the repeating unit = 94.05, Molecular weight of the Cys residue = 120, Molecular weight of one 'H' atom = 1

Similarly, DP of **Cys-PVim-II** was calculated from the ^{1}H-NMR spectrum (see Figure S5) and it was found to be 22.

66.33/3 × 1/1

= 22.11 ≈ 22

Molecular weight (M_n) of **Cys-PVim-II =** (22 × 94.05) + 120 + 1 = 2190.1 ≈ 2200 Da

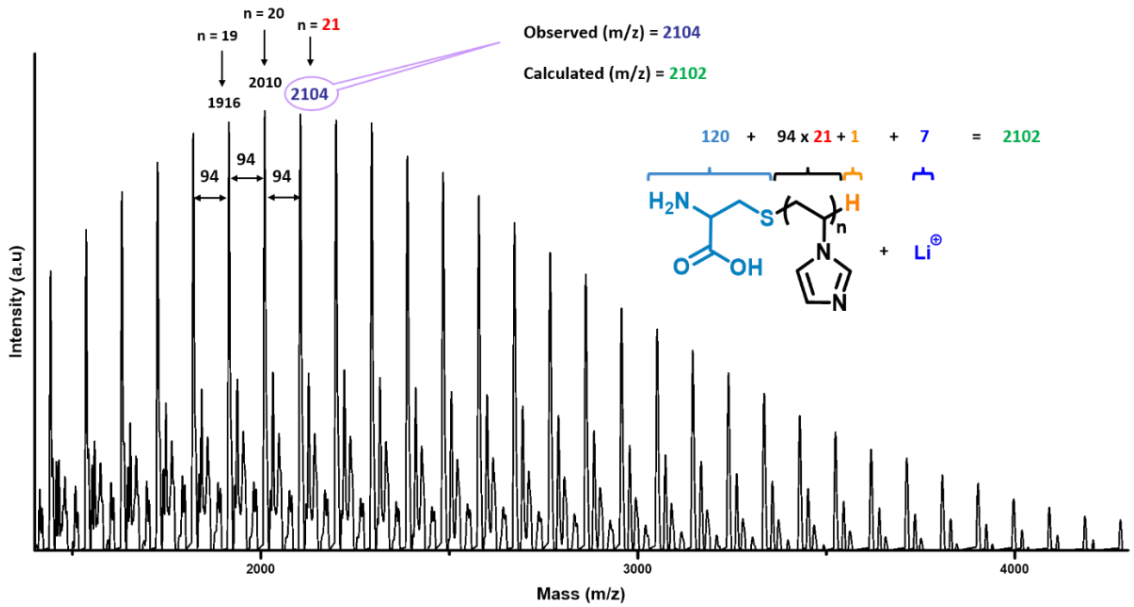

Figure S6. MALDI-TOF-MS spectrum of **Cys-PVim-II** in MeOH using DHB matrix and NaI.

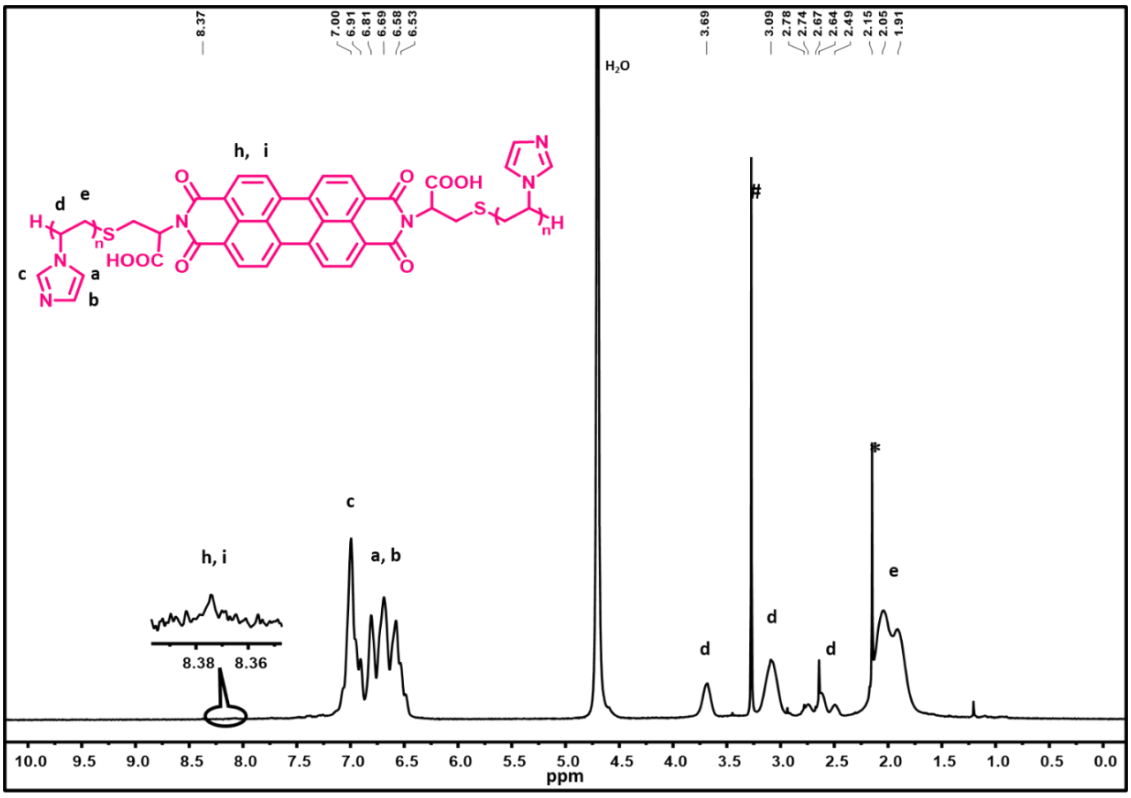

Figure S7. [1]H-NMR spectrum of **PBI-(Cys-PVim-I)$_2$** in D_2O (*for acetone, [#]solvent impurities).

[1]H-NMR (400 MHz, D_2O, TMS, δ ppm), PBI-(Cys-PVim-I)$_2$: 1.72-2.24 (-CH_2 of PVim at position 'e'), 2.43-3.80 (-CH of PVim at position 'd'), 6.42-7.19 (imidazole ring protons at positions 'a', 'b' and 'c'), 7.97-8.20 (aromatic protons of perylene unit at position 'h', 'i').

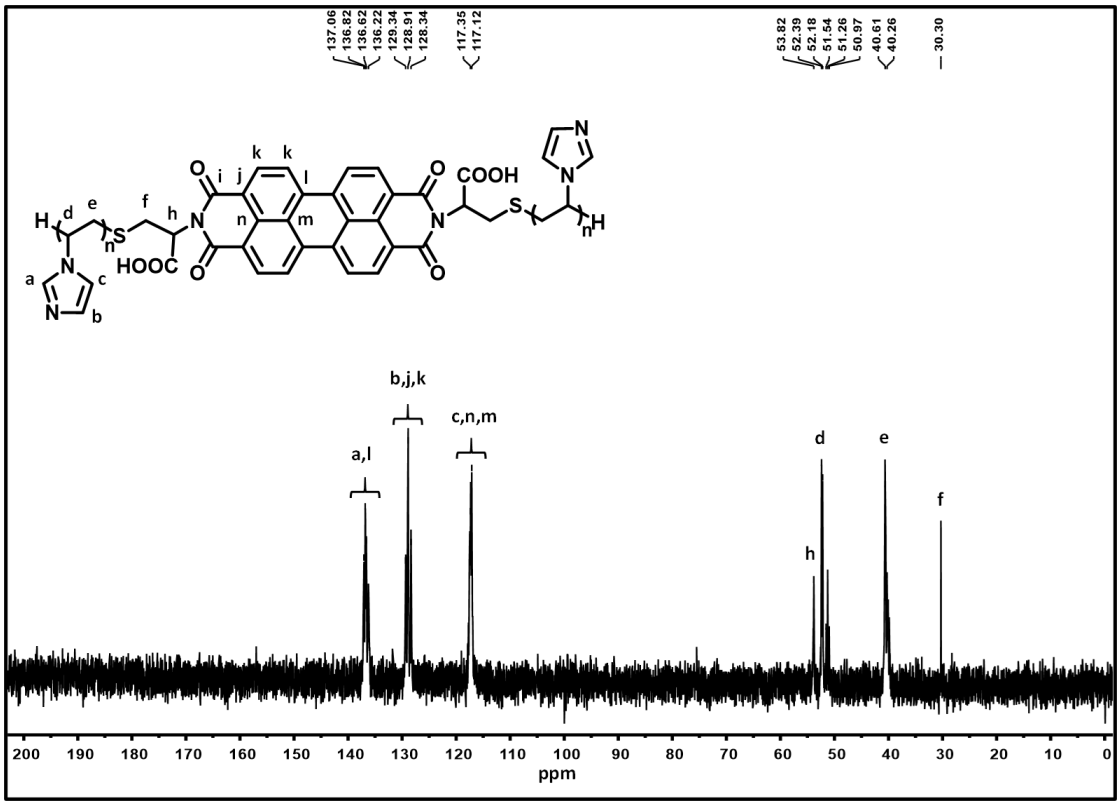

Figure S8. ^{13}C-NMR spectrum of **PBI-(Cys-PVim-I)$_2$** in D_2O.

^{13}C-NMR (100 MHz, D_2O, TMS) (δ, ppm), PBI-(Cys-PVim-I)$_2$: 30.30, 40.26-40.61, 50.97-53.82, 117.12-117.34, 128.34-129.34, 136.22-137.06.

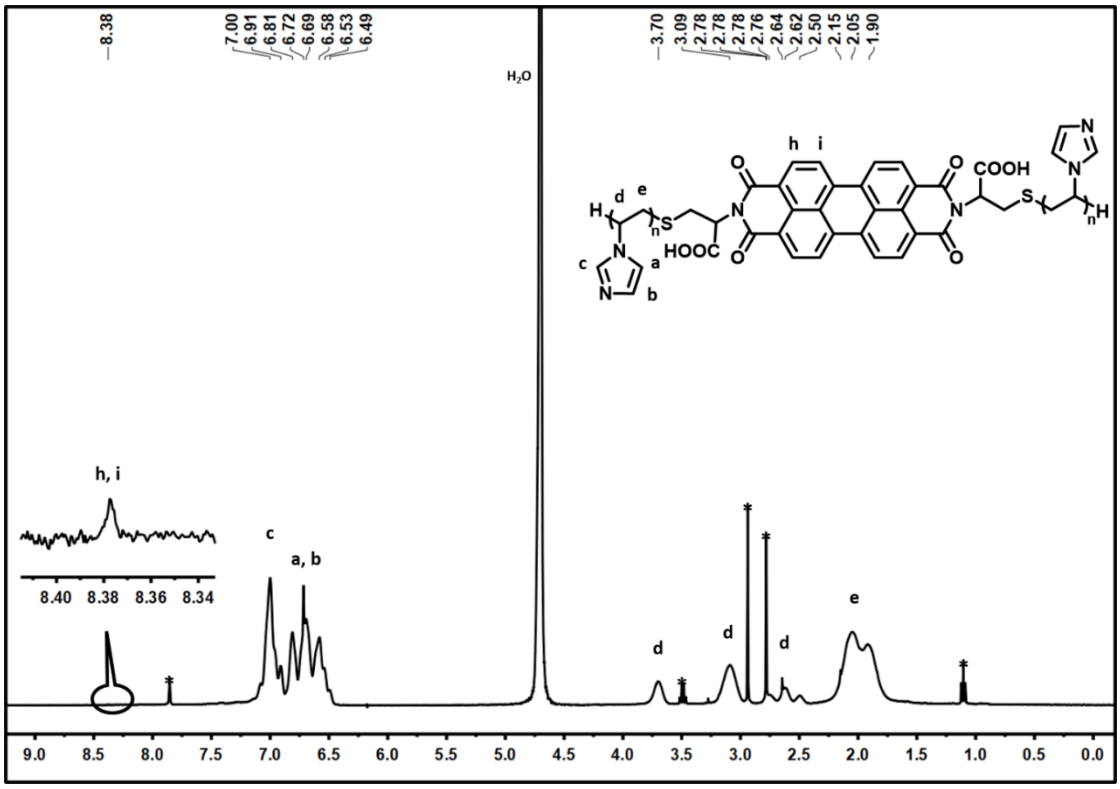

Figure S9. [1]H-NMR spectrum of representative **PBI-(Cys-PVim-II)$_2$** in D_2O (*for DMF).

[1]H-NMR (400 MHz, D_2O, TMS, δ ppm), PBI-(Cys-PVim-II)$_2$: 1.72-2.24 (-CH_2 of PVim at position 'e'), 2.43-3.80 (-CH of PVim at position 'd'), 6.42-7.19 (imidazole ring protons at positions 'a', 'b' and 'c'), 7.97-8.20 (aromatic protons of perylene unit at position 'h', 'i').

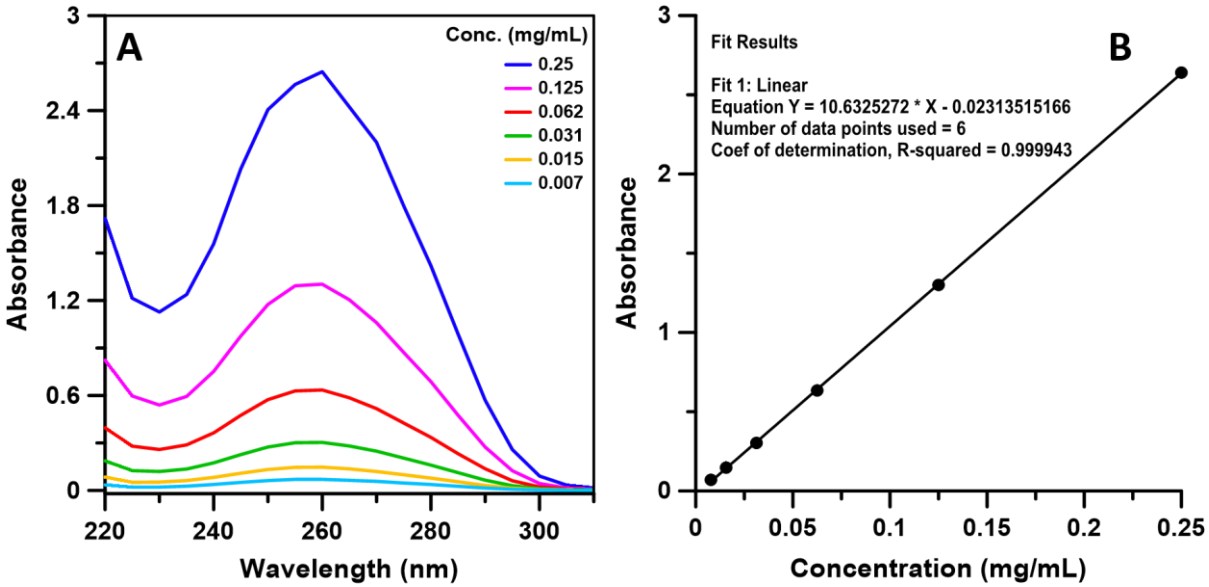

Figure S10. Concentration-dependent UV-vis spectra of ctDNA in 10 mM Tris-HCl buffer (A) and absorbance vs concentration calibration plot showing linear fit (B).

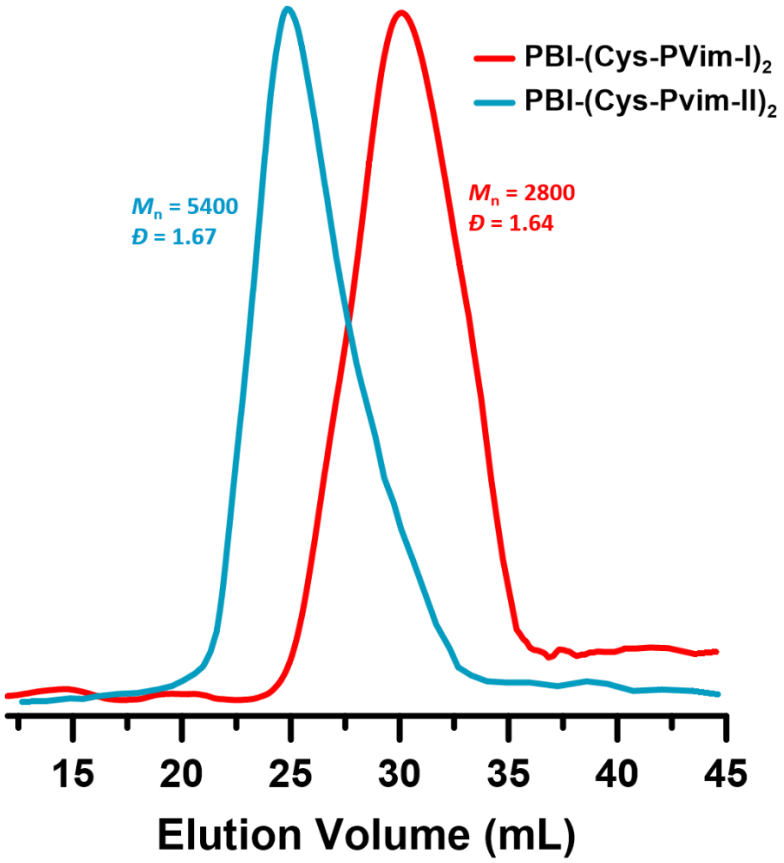

Figure S11. SEC chromatographs of the two different PBI-(Cys-PVim)$_2$ conjugates.

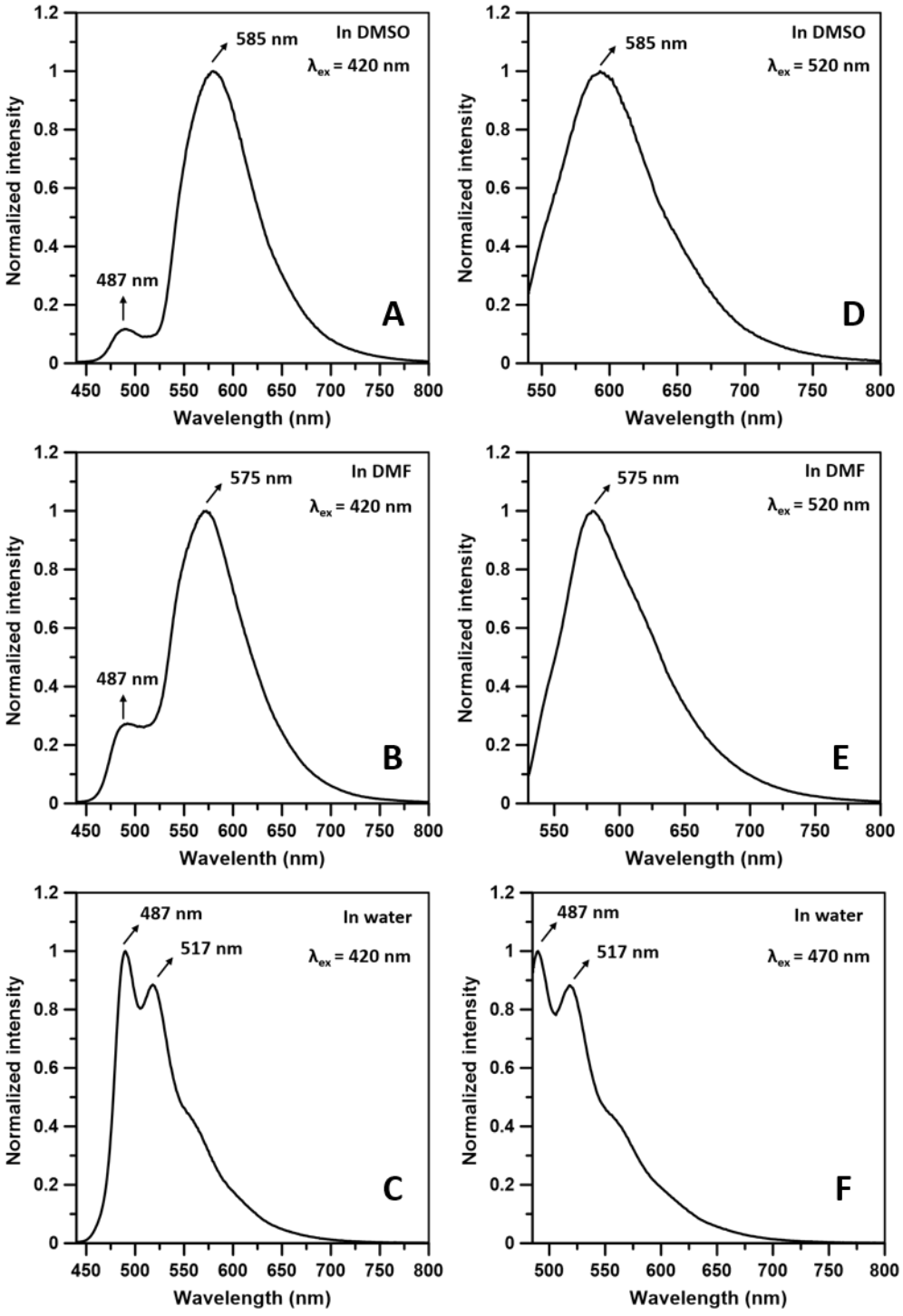

Figure S12. Emission spectra of **PBI-(Cys-PVim-II)$_2$** in DMSO (A and D), DMF (B and E) using the excitation wavelength of 420 nm and 520 nm and in water (C and F) using the excitation wavelengths of 420 and 470 nm.

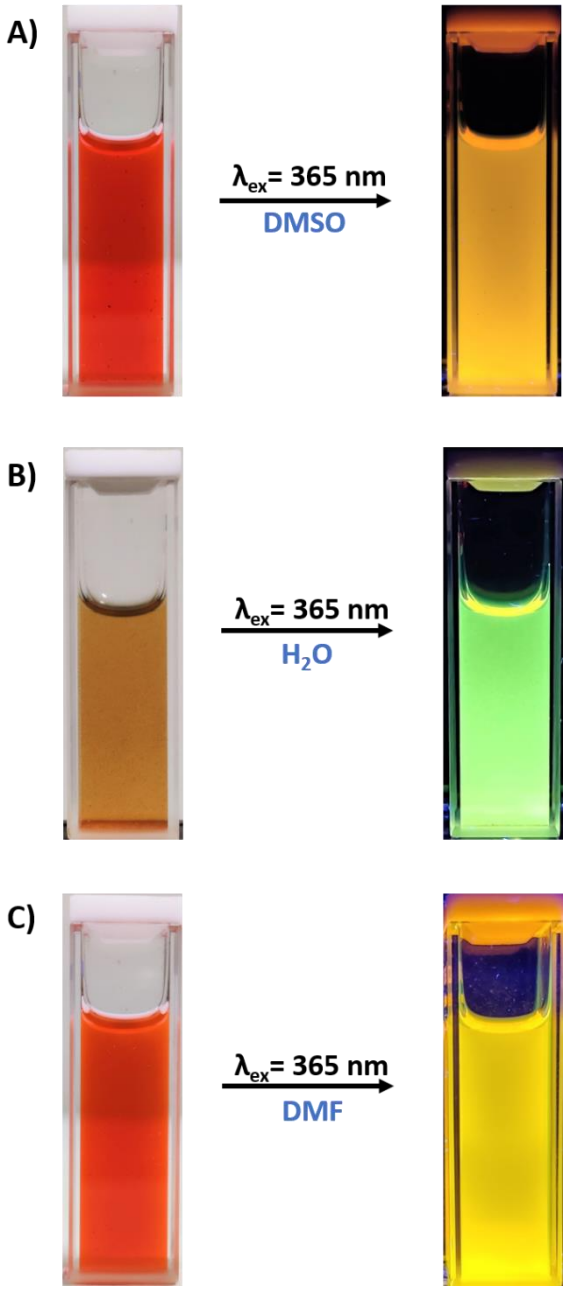

Figure S13. Images of solutions of **PBI-(Cys-PVim-II)$_2$** (1 mg/mL) in A) DMSO (Top), B) water (middle), and C) DMF (bottom) under ambient and UV light.

Quantum yield (ϕ) calculation:

The quantum yield (ϕ) of two PBI-(Cys-PVim)$_2$ conjugates were measured in three different solvents such as DMSO, water and DMF using quinine sulfate as a reference standard and using the following equation.

$$\phi_s = \phi_r [(I/A)_s \times (A/I)_r] \times \eta_s^2/\eta_r^2$$

Where I_s and I_r were the integrated emission peak area of the sample and reference, A_s and A_r were absorbance of the sample and reference at an excitation wavelength of 370 nm. η_s and η_r are the refractive index of the solvent at which the sample and reference were dissolved. ϕ_s and ϕ_r are the quantum yield of the sample and the reference.

ϕ_r of quinine sulfate = 0.53

η_s (DMSO) = 1.47 at 20 ^{o}C, η_s (DMF) = 1.43 at 20 ^{o}C, η_s (water) = 1.33 at 20 ^{o}C

Table S2. Quantum yields (ϕ) of **PBI-(Cys-PVim-I)$_2$** and **PBI-(Cys-PVim-II)$_2$** in DMSO, DMF, and water respectively.

Conjugate sample	ϕ_s in DMSO	ϕ_s in DMF	ϕ_s in water
PBI-(Cys-PVim-I)$_2$	28.2%	38%	19%
PBI-(Cys-PVim-II)$_2$	19.7%	12.8%	15%

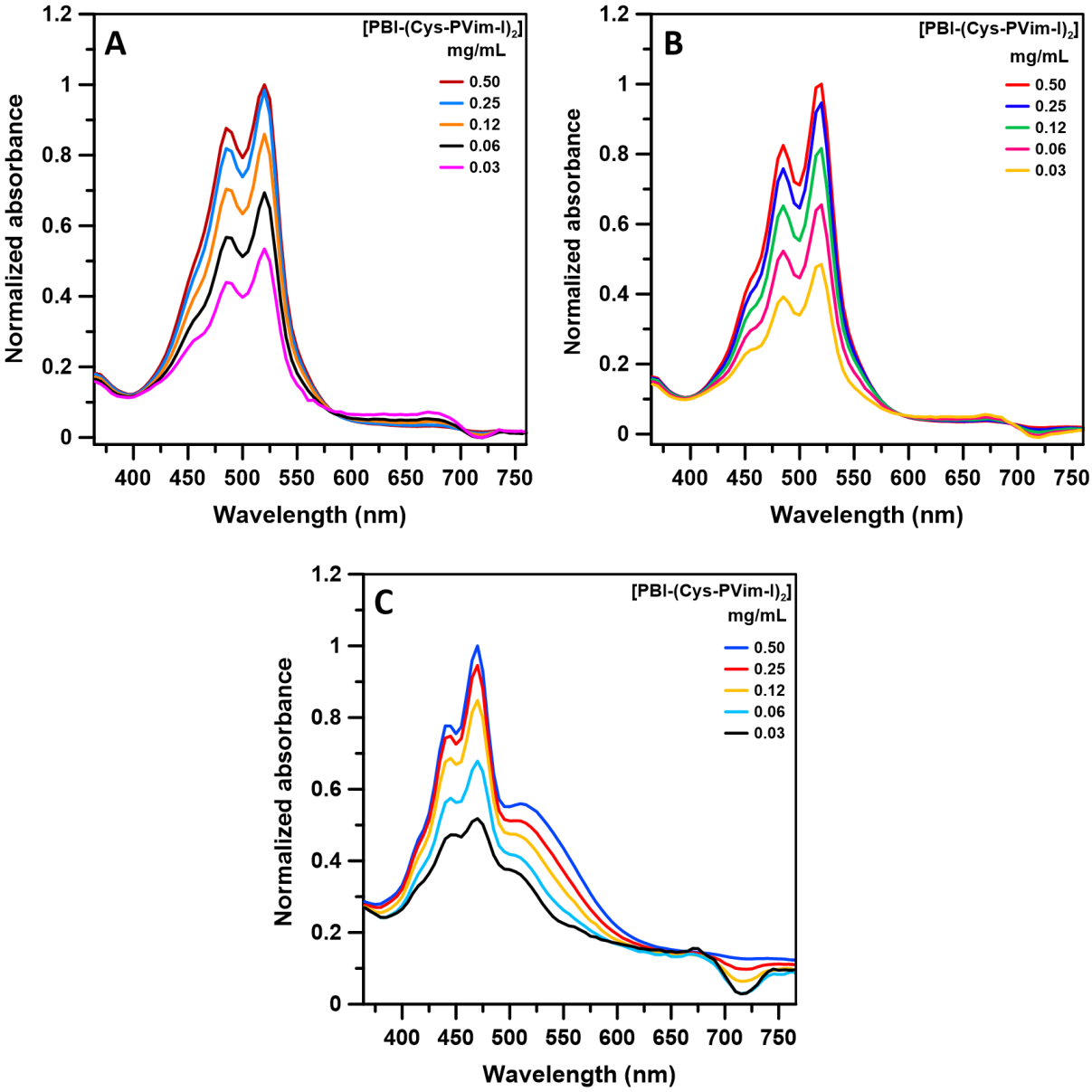

Figure S14. Concentration-dependent UV-vis spectra of **PBI-(Cys-PVim-I)$_2$** conjugate in DMSO (A), DMF (B), and water (C).

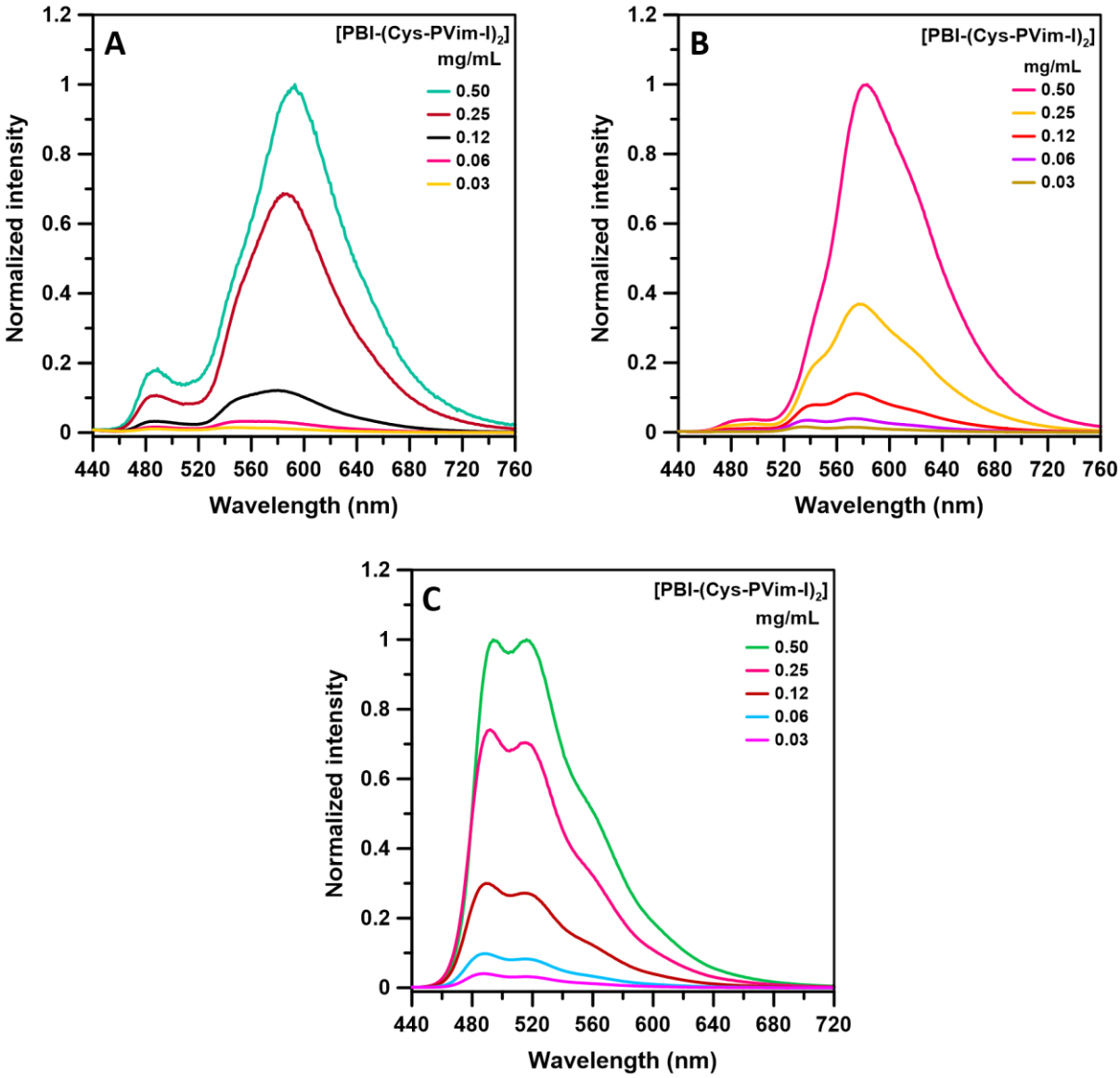

Figure S15. Concentration-dependent emission spectra (λ_{ex} = 420 nm) of **PBI-(Cys-PVim-I)$_2$** in DMSO (A), DMF (B), and water (C).

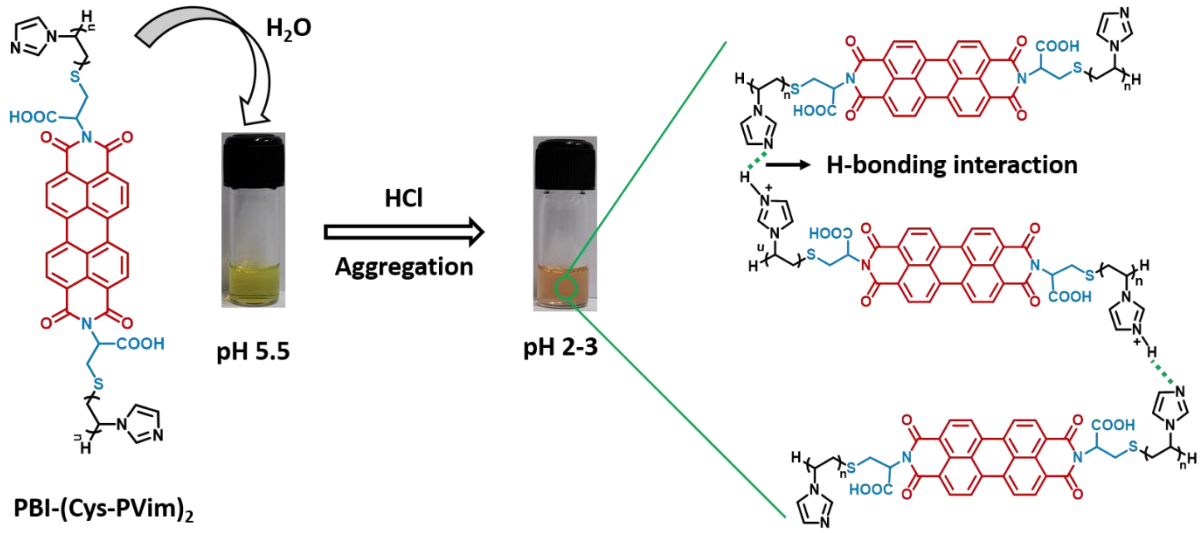

Scheme S1. Schematics of the aggregation between PBI-(Cys-PVim)$_2$ conjugate molecules through H-bonding interactions in acidic medium.

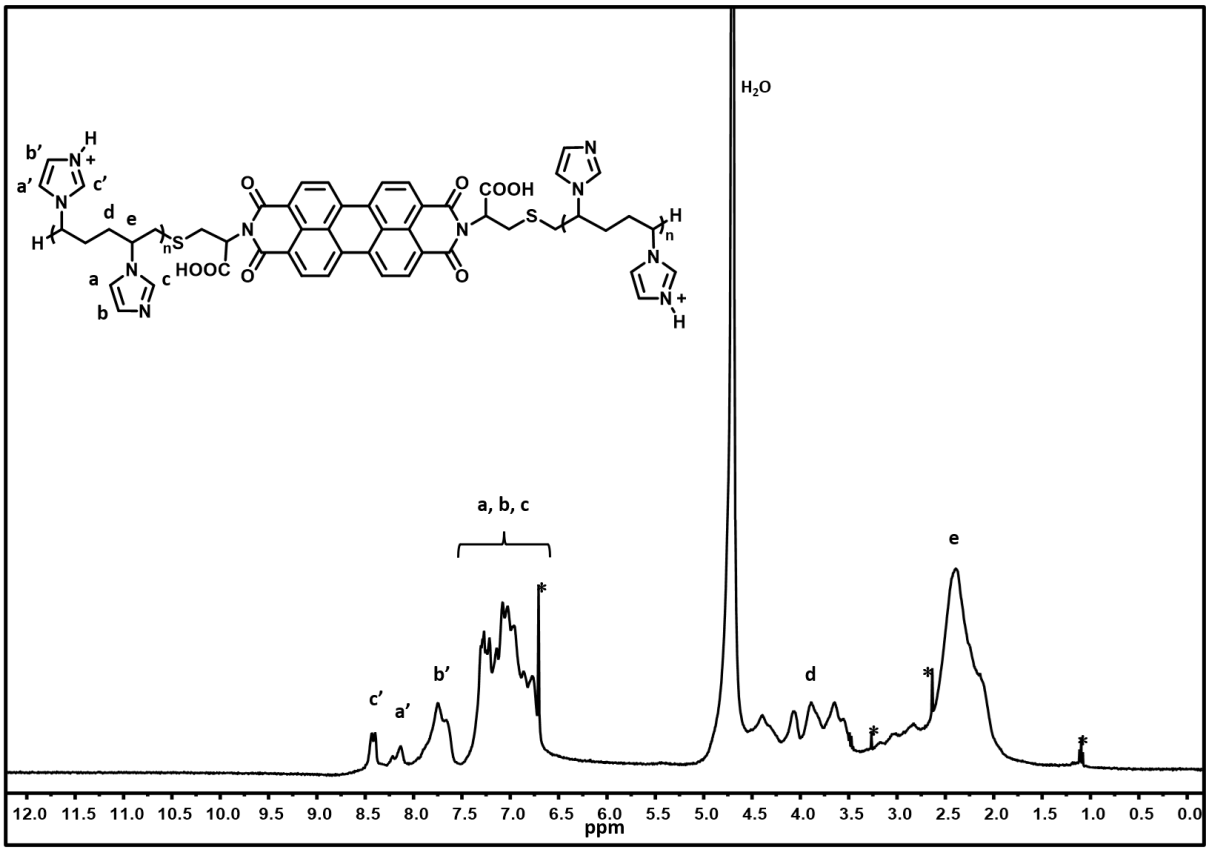

Figure S16. ^{1}H-NMR spectrum of representative **PBI-(Cys-PVim-II)$_2$** in D_2O in presence of HCl (∗solvent impurities).

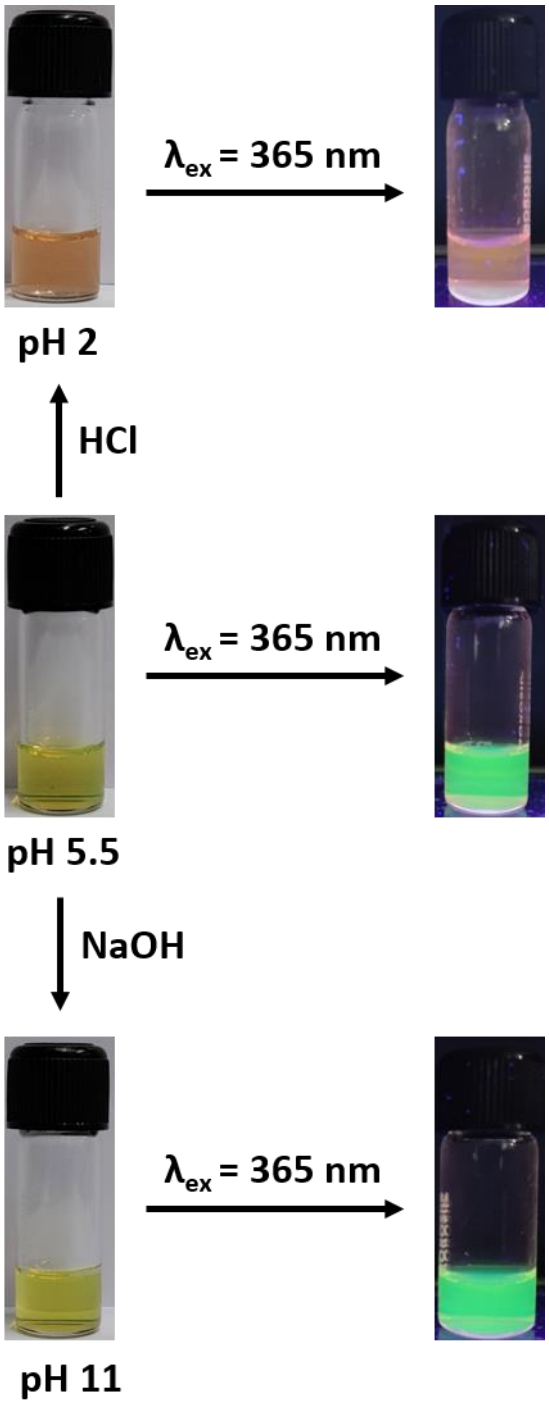

Figure S17. Images of the aqueous **PBI-(Cys-PVim-II)$_2$** solution at different pHs under ambient and under irradiation of UV light.

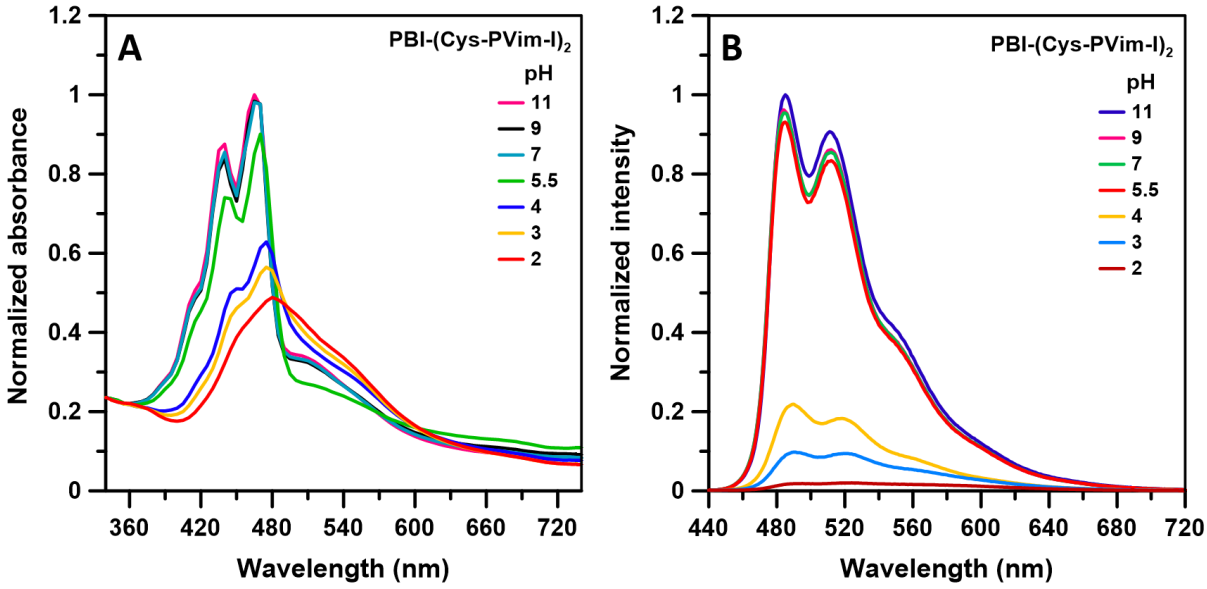

Figure S18. UV-vis absorption (A) and emission (λ_{ex} = 420 nm) (B) spectra of aqueous **PBI-(Cys-PVim-I)$_2$** solution (0.5 mg/mL) at different pH values ranging from 2 to 11.

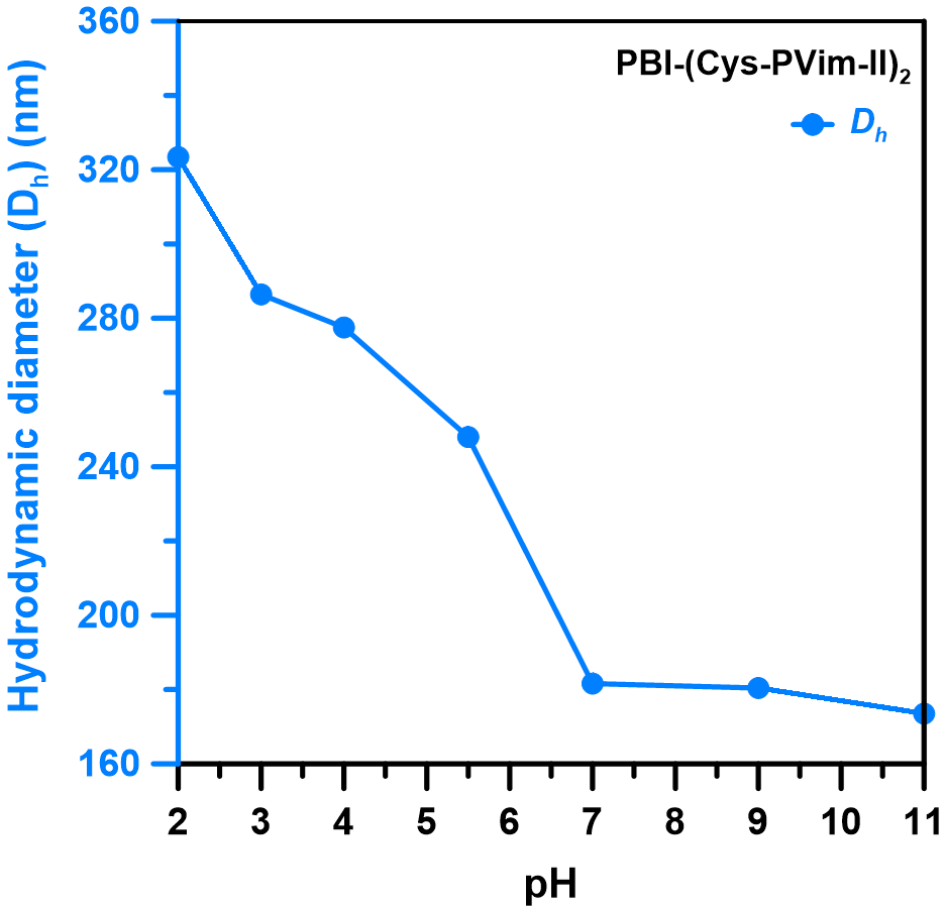

Figure S19. Variation of hydrodynamic diameters (D_hs) of the aqueous solution of **PBI-(Cys-PVim-II)$_2$** (0.5 mg/mL) at different pHs ranging from 2-11.

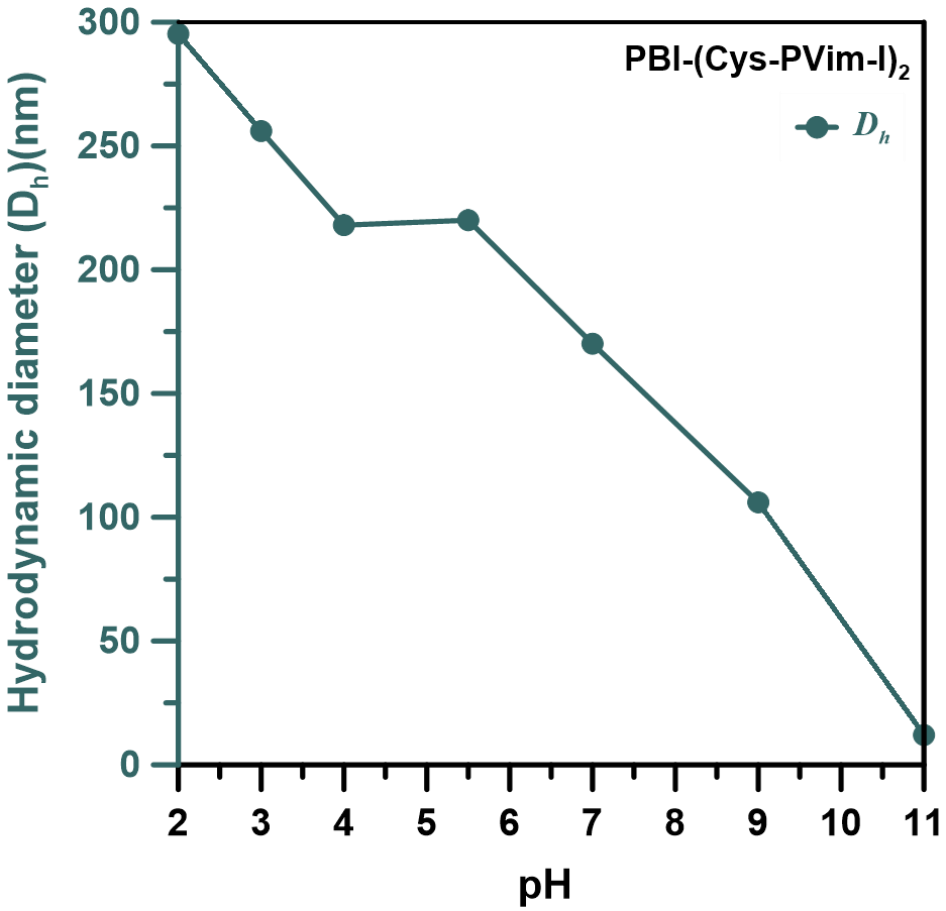

Figure S20. Variation of hydrodynamic diameters (D_hs) of the aqueous solution of **PBI-(Cys-PVim-I)$_2$** (0.5 mg/mL) at different pHs ranging from 2-11.

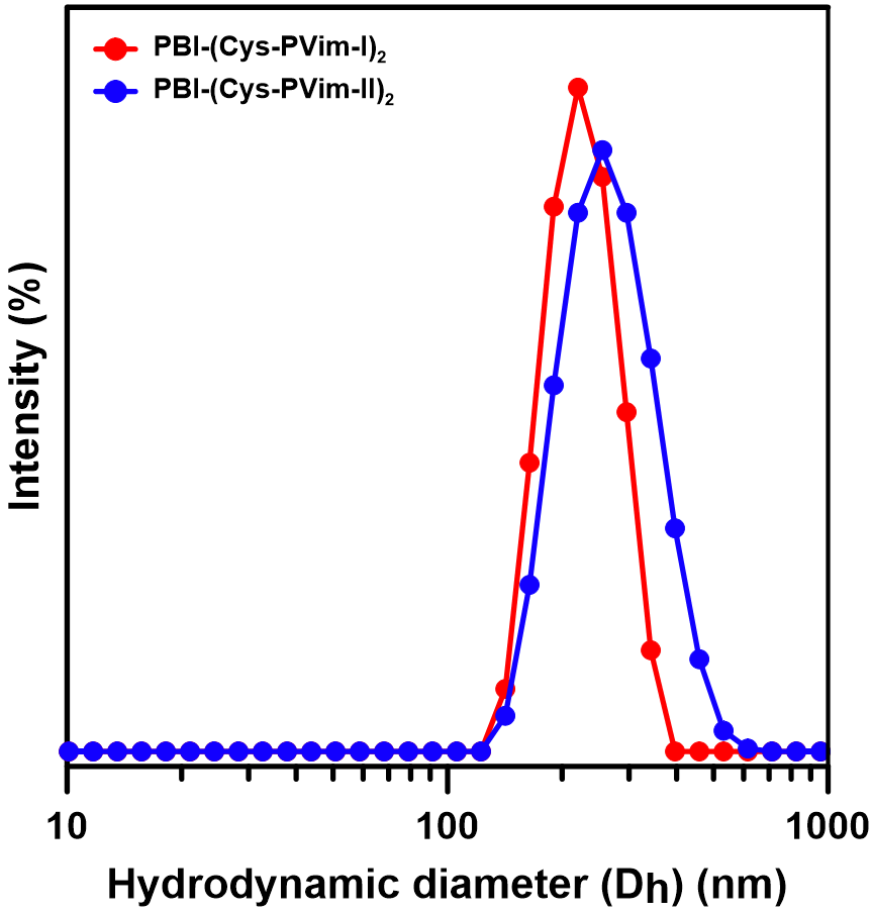

Figure S21. DLS distribution curves of **PBI-(Cys-PVim-I)$_2$** and **PBI-(Cys-PVim-II)$_2$** in water at a concentration of 0.5 mg/mL.

Determination of Critical aggregation concentration (CAC) through DLS:

For CAC measurement, at first a series of aqueous solution of the **PBI-(Cys-PVim-I)$_2$** was prepared with concentrations ranging from 0.06 to 1 mg/mL. The hydrodynamic diameter (D_h) was then measured at 25 °C and were plotted against the logarithm of the concentrations (mg/mL) of polymer solutions. The plot clearly showed a slow increase of D_h with the increase of concentration followed by a sudden jump. The CAC was measured at which the D_h was half of its maximum value and was found to be 0.44 mg/mL (Figure S22).

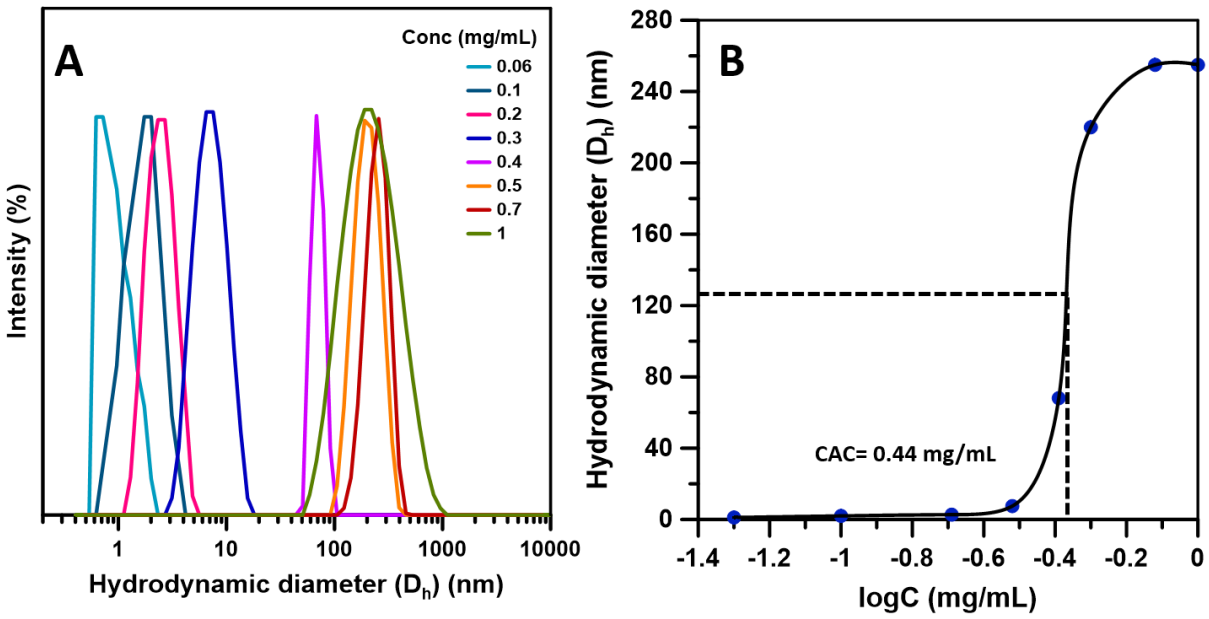

Figure S22. Particle size distribution of the **PBI-(Cys-PVim-I)$_2$** in water of its varying concentration ranging from (0.06 to 1 mg/mL) (A). The plot of D_h as a function of logarithm of **PBI-(Cys-PVim-I)$_2$** concentration.

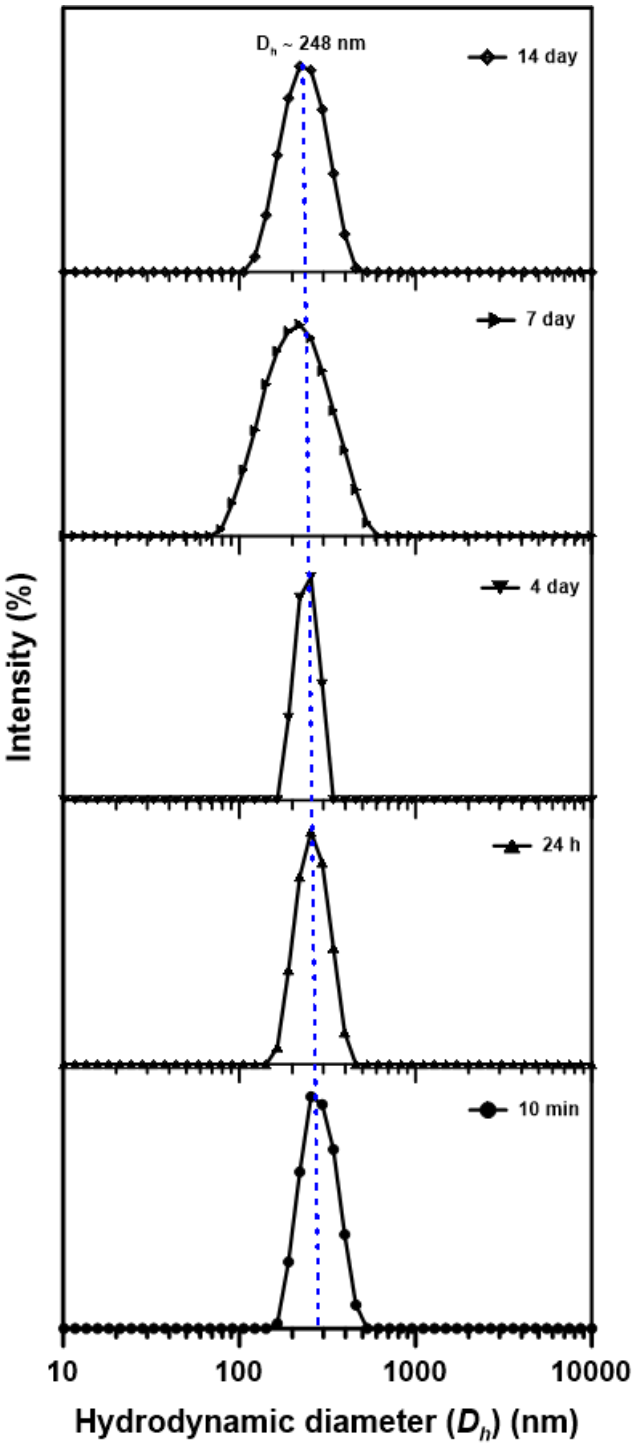

Figure S23. DLS distribution curves of **PBI-(Cys-PVim-II)$_2$** (0.5 mg/mL) in water at different time intervals.

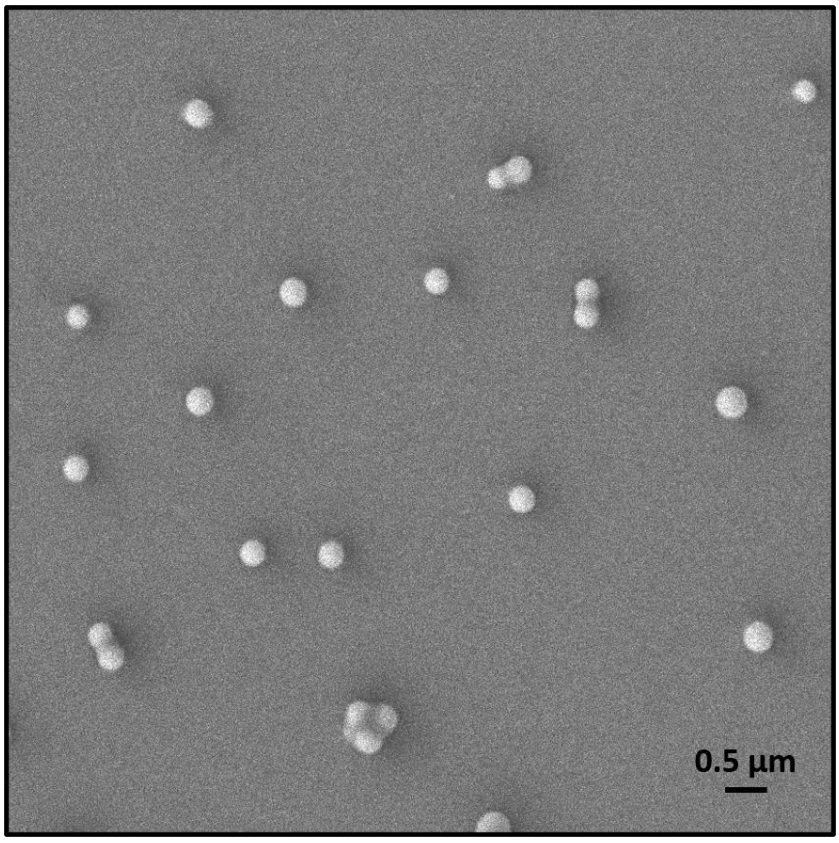

Figure S24. FESEM image of aggregated **PBI-(Cys-PVim-II)$_2$** formed in water at a concentration of 0.5 mg/mL.

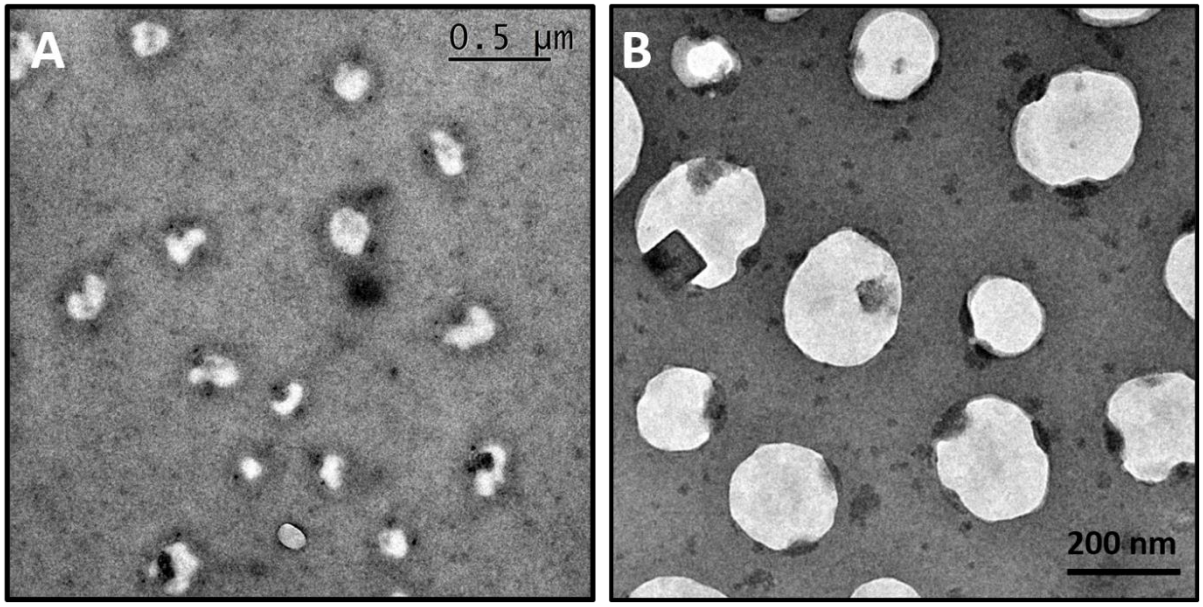

Figure S25. TEM images of vesicular aggregates of **PBI-(Cys-PVim-I)$_2$** (A) and **PBI-(Cys-PVim-II)$_2$** in water at a concentration of 0.5 mg/mL.

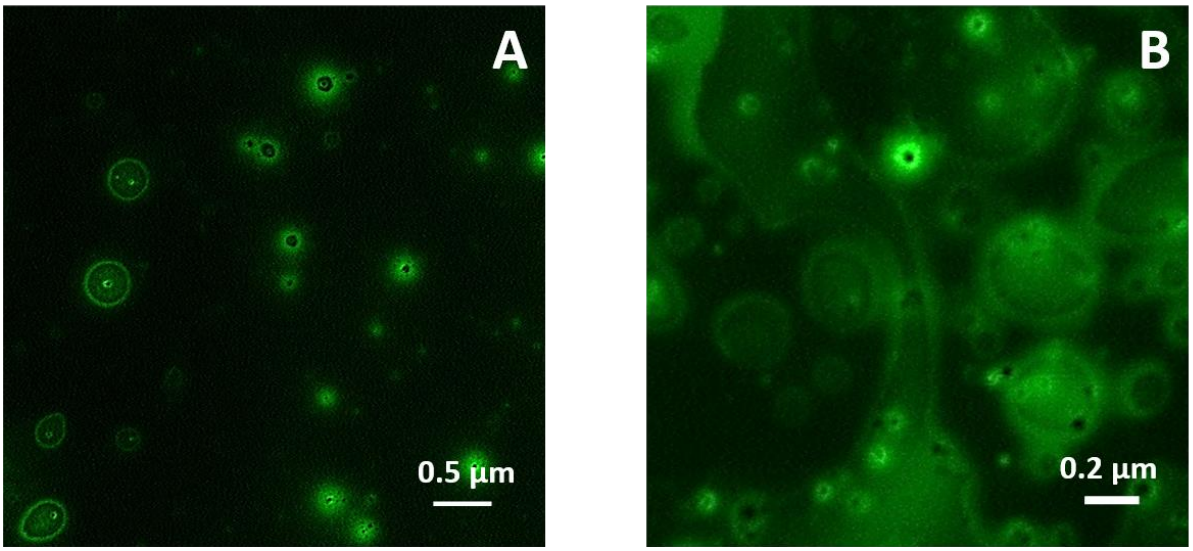

Figure S26. Confocal microscopic images of vesicular aggregates of **PBI-(Cys-PVim-II)$_2$** (A) and **PBI-(Cys-PVim-I)$_2$** (B) in water at a concentration of 0.5 mg/mL.

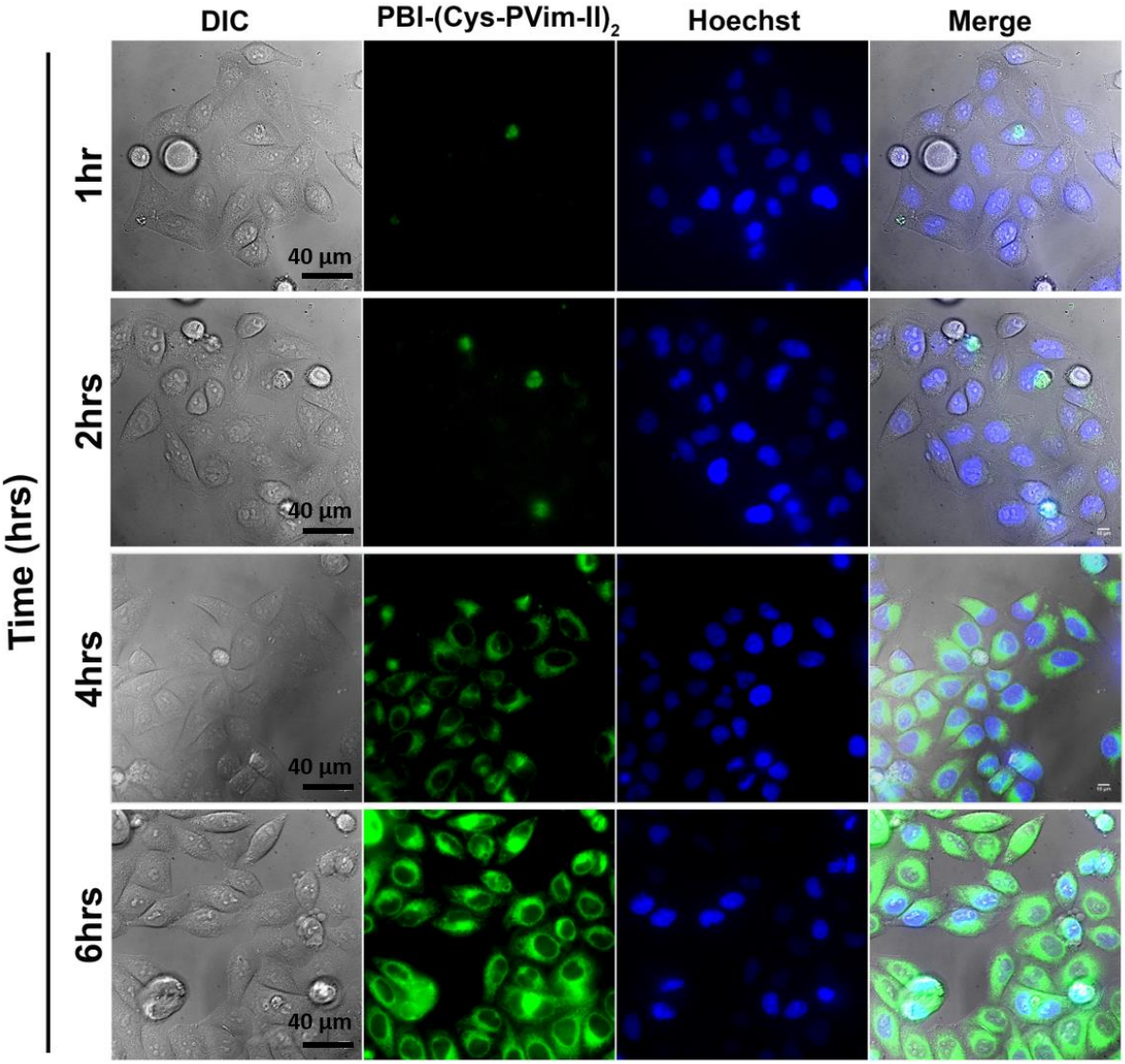

Figure S27. Time-dependent fluorescence microscopic live cell images of HeLa cells in the presence of **PBI-(Cys-PVim-II)$_2$** conjugate.

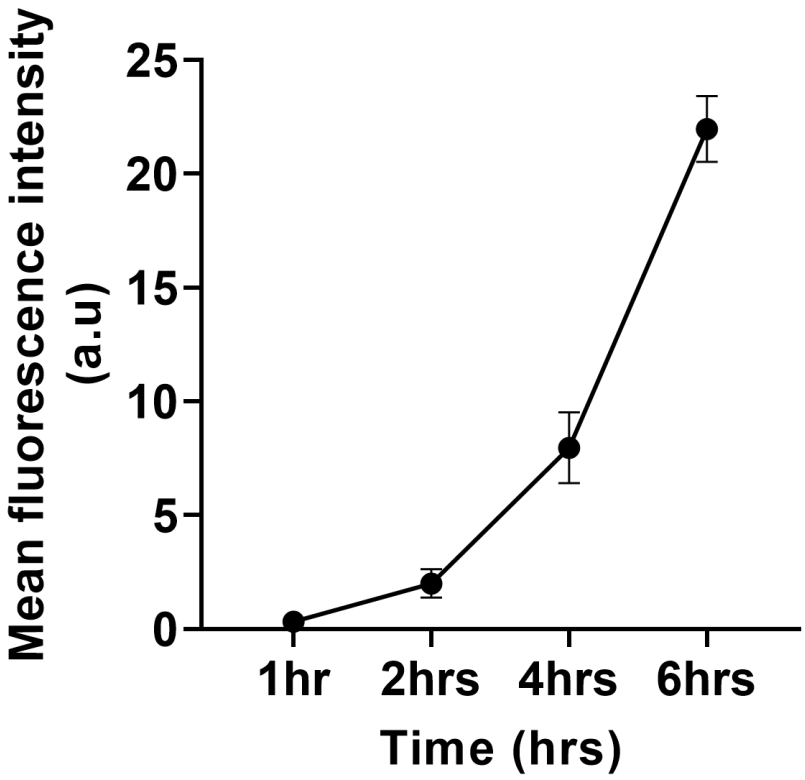

Figure S28. Variation of mean fluorescence intensity with increasing the incubation time of HeLa cells in the presence of **PBI-(Cys-PVim-II)$_2$**.

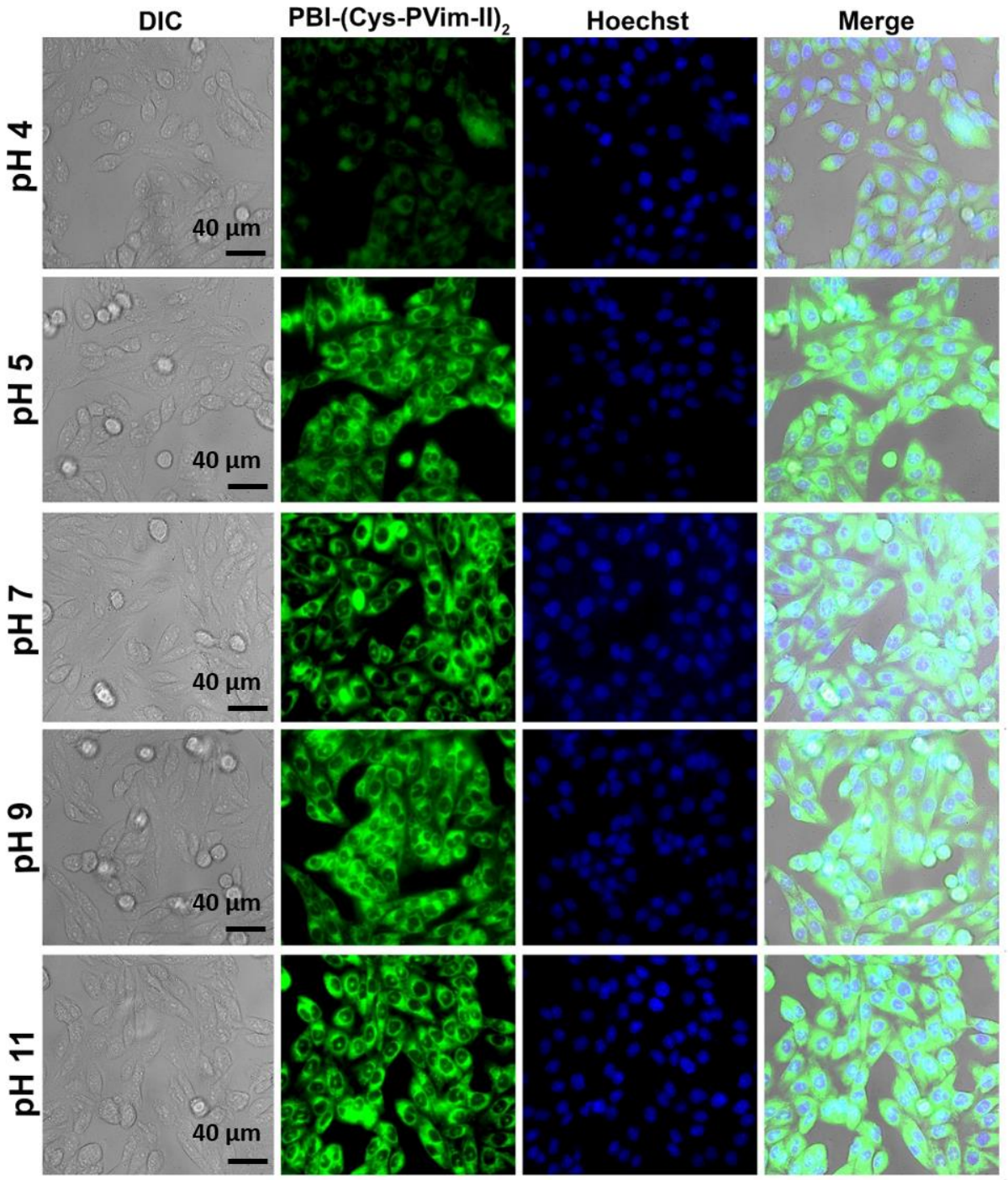

Figure S29. pH-dependent fluorescence microscopic live cell images of HeLa cells in the presence of **PBI-(Cys-PVim-II)$_2$** conjugate.

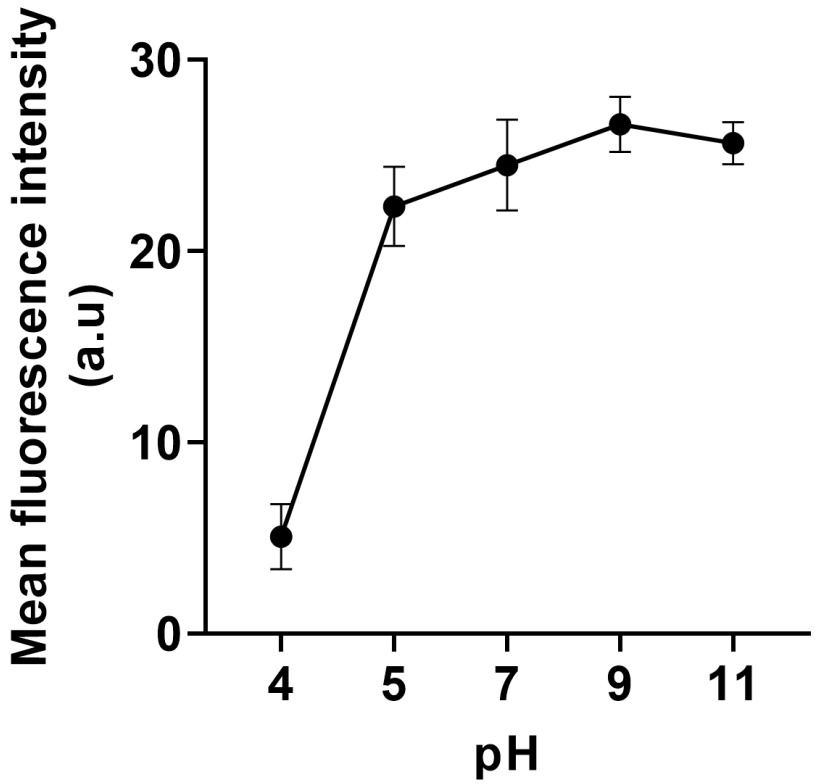

Figure S30. Variation of mean fluorescence intensity with increasing the pH of incubated HeLa cells in the presence of **PBI-(Cys-PVim-II)$_2$**.

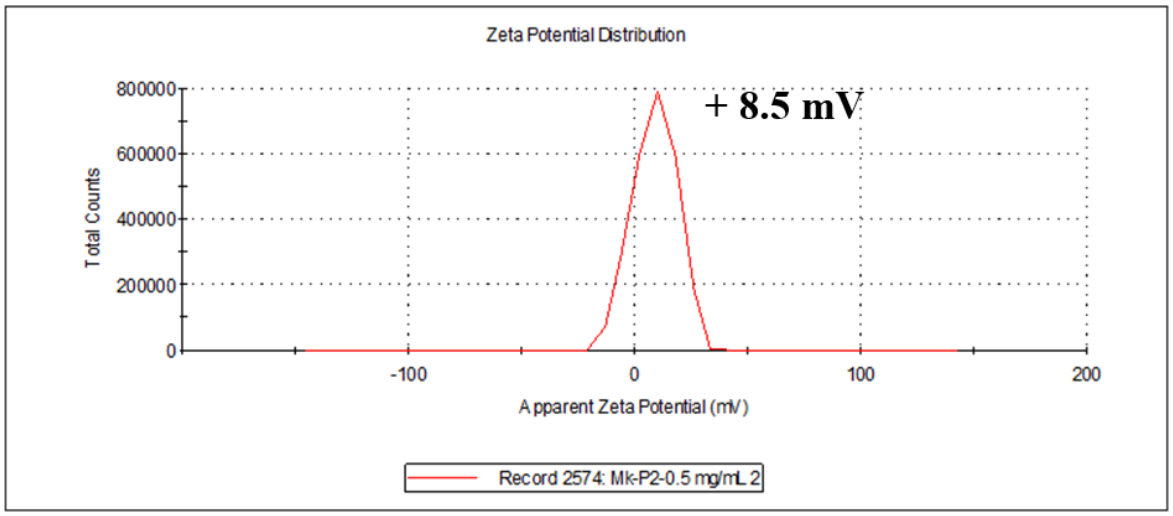

Figure S31. Zeta potential (ξ) of **PBI-(Cys-PVim-II)$_2$** conjugate in water at a concentration of 0.5 mg/mL.

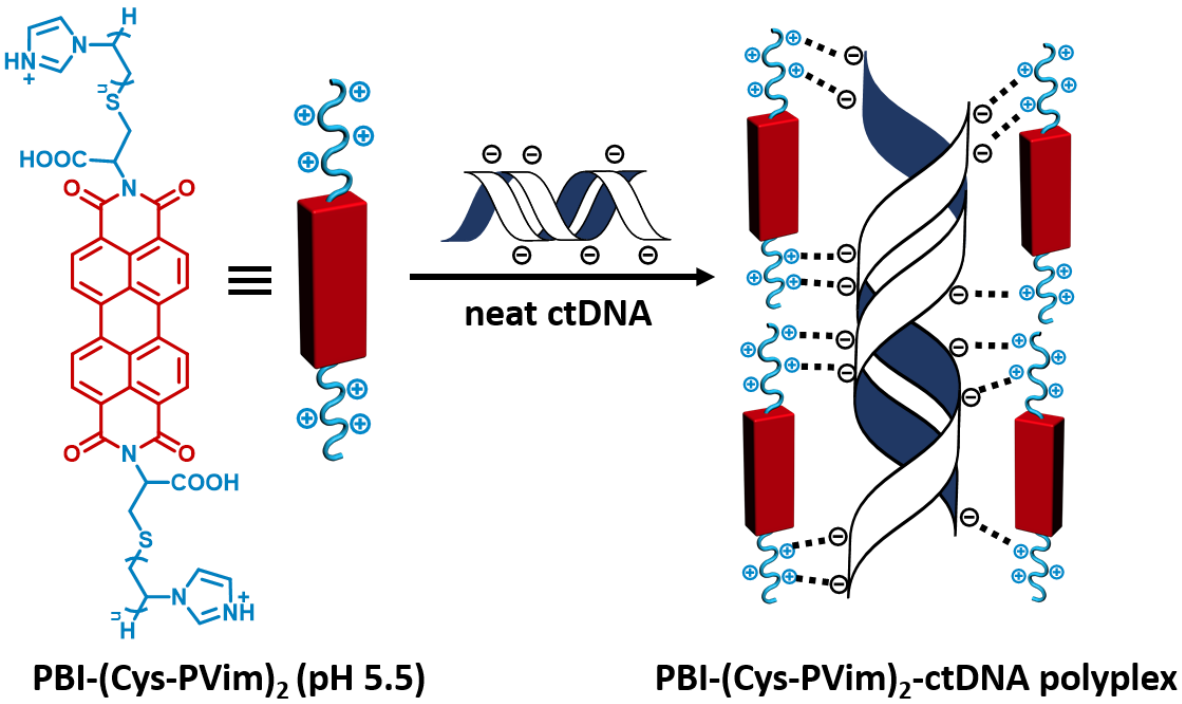

Scheme S2. Schematic representation for the binding of ctDNA with PBI-(Cys-PVim)$_2$ conjugate.

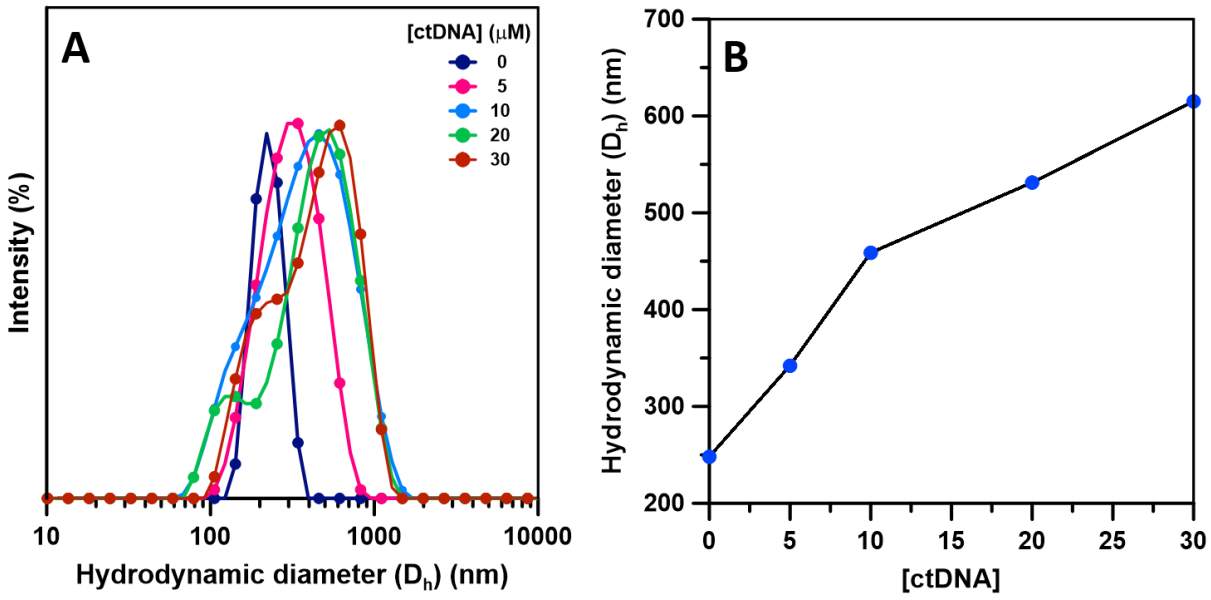

Figure S32. Intensity-weighted particle size-distribution of **PBI-(Cys-PVim-II)$_2$** (35 μM) with different concentrations of ctDNA (A). The plot of variation of hydrodynamic diameters (D_hs) of **PBI-(Cys-PVim-II)$_2$**/ctDNA polyplexs in the presence of varying concentration of ctDNA (B).

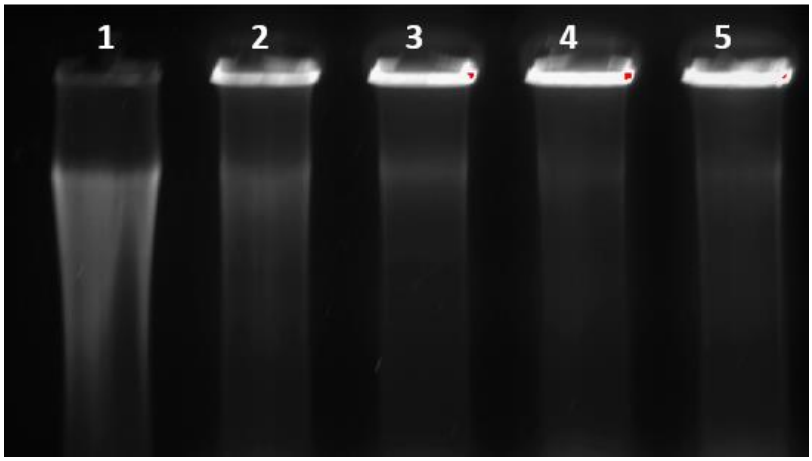

Figure S33. Electrophoretic mobility of ctDNA (1.27 mM) upon addition of different concentrations of **PBI-(Cys-PVim-II)**$_2$ ranging from 35-80 μM.

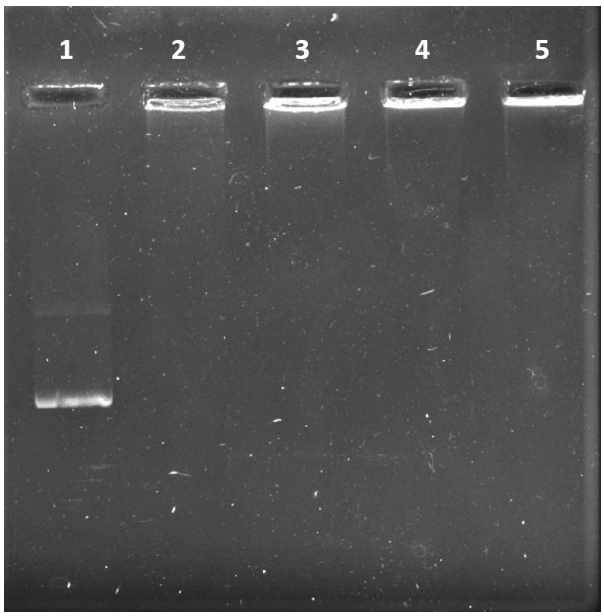

Figure S34. Electrophoretic mobility of plasmid DNA (100 ng/mL) upon addition of different concentrations of **PBI-(Cys-PVim-II)$_2$** ranging from 35-80 μM**.**

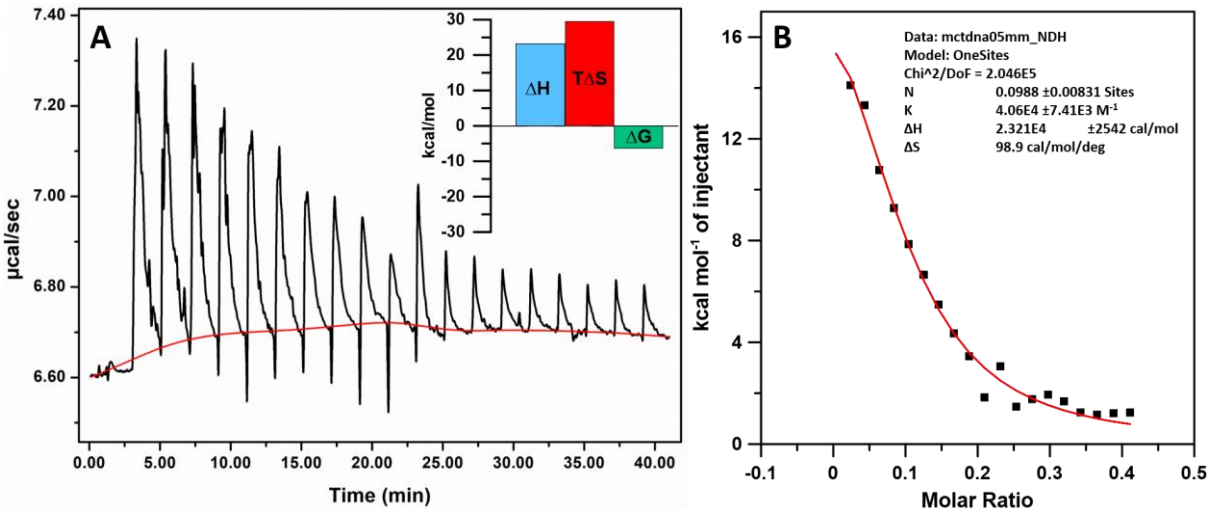

Figure S35. ITC thermogram showing the titration of 1 mM of ctDNA with 0.5 mM of **PBI-(Cys-PVim-II)$_2$**, Inset showed the comparison of the enthalpy, entropic factor, and the Gibbs energy of the interactions (A). The one-site binding plotting from the thermogram (B)